J. Fluid Mech. (1996), *vol.* 314, *pp.* 267–297

Classification of self-organized vortices in two-dimensional turbulence: the case of a bounded domain

By P. H. CHAVANIS AND J. SOMMERIA
Ecole Normale Supérieure de Lyon, 69364 Lyon cedex 07, France

(Received 17 April 1995 and in revised form 3 January 1996)

We calculate steady solutions of the Euler equations for any given value of energy and circulation (and angular momentum in the case of a circular domain). A linear relationship between vorticity and stream function is assumed. These solutions correspond to the predicted self-organization into a maximum-entropy state, in the limit of strong mixing. Vorticity mixing is then only weakly restricted by the constraint of energy conservation. While maximum-entropy solutions depend in general on the whole probability distribution of vorticity levels, these linearized results depend only on a single control parameter, yet keeping much of the general structure of the problem. A convenient classification of the maximum-entropy states is thus provided. We show furthermore how to extend these linearized results as an expansion in energy, involving successive moments of the vorticity probability distribution. They are applied to a rectangular domain and compared with existing numerical and laboratory results. We predict that the flow organizes into a single vortex in the square domain, but into a two-vortex dipolar state in a rectangle with aspect ratio greater than 1.12. The case of a circular domain is also explicitly solved, taking into account the conservation of the angular momentum.

1. Introduction

The formation of coherent structures is a remarkable property of two-dimensional turbulence. Such organization is observed in large-scale oceanic or atmospheric flows, and can be reproduced in laboratory experiments and numerical simulations. A general explanation of this organization has been proposed by Onsager (1949), in terms of equilibrium statistical mechanics for a set of point vortices. This is a remarkable anticipation since observations were very scarce at that time. This idea has been further developed by Joyce & Montgomery (1973) and Montgomery & Joyce (1974), who have obtained more explicit predictions by a mean field approximation. The result appears as a relationship between the locally averaged vorticity and stream function, which selects a steady solution of the Euler equations. However, this prediction depends on the distribution of the strengths of the point vortices used to model the initial state, so it is not unique. It can lead to inconsistencies: in particular the maximum vorticity is not bounded by the initial maximum, as it should be for the two-dimensional Euler equations.

A solution to this problem was proposed by Kuz'min (1982), then rediscovered and further developed by Robert (1990) and Robert & Sommeria (1991), and independently by Miller (1990). This equilibrium statistical theory is applied directly

to the continuous Euler equations, developing ideas first proposed in the context of the Vlasov equation by Lynden-Bell (1967). In this case the standard procedure for Hamiltonian systems of particles is not available, but still the method is justified (on a weaker basis) by a set of rigorous properties (Robert 1991; Michel & Robert 1994). The result is again a steady solution of the Euler equations, on which fine-scale vorticity fluctuations are superimposed. The relationship between vorticity and stream function is different than in Montgomery & Joyce (1974), and it is now quite consistent with the properties of the continuous Euler equations.

This theory provides in principle a well-defined prediction for the final organization of a perfect fluid with any initial condition and shape of the fluid domain. However, the practical determination of the equilibrium flow is generally difficult; it requires solution of a nonlinear partial differential equation, with unknown coefficients, given only indirectly through integral constraints, corresponding to the conserved quantities. Different numerical methods have been developed to solve this problem (Pointin & Lundgren 1976; Smith & O'Neil 1990; Whitaker & Turkington 1994), but still the solutions must be classified according to several bifurcation parameters, and it is often difficult to unravel the structure of the bifurcation diagram, except for the most simple cases.

The present paper provides a general approach to classify these optimal solutions. The idea is to linearize the relationship between vorticity and stream function, which appears to be valid in a limit of strong mixing. The solutions can be then related to the eigenfunctions of the Laplacian in the fluid domain. Although the partial differential equation is linearized, the problem is still nonlinear due to the constraint on energy, and a rich bifurcation diagram is already obtained in this approximation, and provides the skeleton for the more general problem. While the optimal structure depends in principle on the whole distribution of vorticity levels, the linearized solutions depend only on the circulation and enstrophy. This can be considered as the first term in an expansion of the solution in terms of the successive moments of the vorticity distribution. The idea of this expansion has been already sketched in Sommeria (1994), and it is here systematically developed.

Of course the determination of particular solutions of the Euler equations involving a linear relationship between vorticity and stream function is an old idea. The dipole translating in inviscid fluid is a well-known example (Chaplygin 1902), as well as its quasi-geostrophic generalization, called a modon (Stern 1975). The model of Fofonoff (1954) for inertial oceanic circulation is another example in the quasi-geostrophic context. Such examples are particular families of solutions depending on some parameters. In the present paper, we seek instead the linearized solution corresponding to a given set of *integral constraints* (expressing the conserved quantities of the system). It is therefore an actual prediction of the flow organization from a class of initial states, not just an example of steady solution.

We first recall in §2 the principle of the statistical theory, in the general case of any continuous vorticity distribution, and explain our expansion procedure for strong mixing. The general solutions of the linearized problem are given in §3, in term of the eigenmodes of the Laplacian in the fluid domain. Several general solutions are obtained for a given set of integral constraints, and they must be classified by their entropy, as discussed in §3.4. Most solutions with lower entropy are not even local entropy maxima and can be eliminated, as stated in §3.5. As an illustration of this general derivation, we consider in §4 the example of a rectangular domain with various aspect ratios.

For domains with translational or rotational symmetry, a specific adaptation of the general method is necessary, taking into account the corresponding additional conserved quantities. The case of a channel, where the momentum is conserved, has been numerically studied by Thess, Sommeria & Juttner (1994) and Juttner, Thess & Sommeria (1995). In the limit of strong mixing, linearization has led to explicit solutions like in the present paper. The case of a disk, where angular momentum is conserved, is analysed in §5, and explicitly solved in the limit of strong mixing. The case of an infinite domain, with both translational and rotational symmetries, is also of particular interest. However it requires specific developments, due to the self-confinement of the vorticity structures in a sub-domain with free boundaries, and it will be the subject of a second related paper (Chavanis & Sommeria 1996).

Finally we show in §6 that in the linearized limit, our results are in agreement with a form of selective decay hypothesis: the system organizes into the minimal-enstrophy state for a given energy (see e.g. Kraichnan & Montgomery 1980; Hasegawa 1985).

2. The statistical theory: general case and the linearized limit

2.1. *General principles and notation*

The Euler equations are known to develop very complex vorticity filaments, and a deterministic descripition of the flow would require a rapidly increasing amount of information as time goes on. Following Robert & Sommeria (1991), we develop instead a macroscopic description of the system in terms of local probability distributions of the different vorticity levels (called Young's measures in mathematics).

A macroscopic state is defined by the probability $\rho(\boldsymbol{r}, \sigma)$ of finding the vorticity level σ in a small neighbourhood of the position $\boldsymbol{r}$. The normalization condition yields at each point

$$\int \rho(\boldsymbol{r}, \sigma)\mathrm{d}\sigma = 1. \tag{2.1}$$

The locally averaged field of vorticity is expressed in terms of the probability density in the form

$$\overline{\omega}(\boldsymbol{r}) = \int \rho(\boldsymbol{r}, \sigma)\sigma\mathrm{d}\sigma. \tag{2.2}$$

This locally averaged field is called the macroscopic, or coarse-grained, vorticity field. The associated (macroscopic) stream function satisfies in the fluid domain ($\mathscr{D}$)

$$\overline{\omega} = -\Delta\psi \quad \text{with} \quad \psi = 0 \quad \text{on} \quad (\partial\mathscr{D}). \tag{2.3}$$

It is then possible to express the conserved quantities as integrals of the macroscopic fields. These conserved quantities are the energy:

$$E = \frac{1}{2}\int \psi\overline{\omega}\mathrm{d}^2\boldsymbol{r} \tag{2.4}$$

and the global probability distribution of vorticity $\gamma(\sigma)$ (i.e. the total area of each vorticity level):

$$\gamma(\sigma) = \int \rho(\boldsymbol{r}, \sigma)\mathrm{d}^2\boldsymbol{r}. \tag{2.5}$$

In particular the different moments of the vorticity:

$$\Gamma_n = \int \gamma(\sigma)\sigma^n\mathrm{d}\sigma = \int \overline{\omega^n}\mathrm{d}^2\boldsymbol{r} \tag{2.6}$$

are conserved. The first-order moment $\Gamma \equiv \Gamma_1$ is the circulation while the second-order moment Γ_2 is the (fine-grained) enstrophy. In a domain with rotational or translational symmetries, additional quantities are conserved, like the angular momentum in the disk (see §5).

The most probable macroscopic state is obtained by maximizing the entropy:

$$S = -\int \rho(\boldsymbol{r},\sigma)\ln\rho(\boldsymbol{r},\sigma)\mathrm{d}^2\boldsymbol{r}\mathrm{d}\sigma, \tag{2.7}$$

with the constraints (2.1) (2.4) and (2.5) brought by the conserved quantities (and the normalization). This variational problem is treated by introducing Lagrange multipliers so that the first variations satisfy

$$\delta S - \tilde{\beta}\,\delta E - \int \tilde{\alpha}(\sigma)\,\delta\gamma(\sigma)\,\mathrm{d}\sigma - \int \tilde{\zeta}(\boldsymbol{r})\,\delta\left(\int \rho(\boldsymbol{r},\sigma)\mathrm{d}\sigma\right)\mathrm{d}^2\boldsymbol{r} = 0 \tag{2.8}$$

where $\tilde{\beta}$ is the inverse temperature and $\tilde{\alpha}(\sigma)$ the 'chemical potential' of species σ. The resulting optimal probability density $\rho(\boldsymbol{r},\sigma)$ is related to the equilibrium stream function ψ by the relationship (see Robert & Sommeria 1991)

$$\rho(\boldsymbol{r},\sigma) = \frac{1}{Z(\psi)}g(\sigma)\,\mathrm{e}^{-\tilde{\beta}\sigma\psi} \tag{2.9}$$

where $g(\sigma) = \mathrm{e}^{-\tilde{\alpha}(\sigma)}$ and $Z(\psi) = \mathrm{e}^{\tilde{\zeta}(\boldsymbol{r})}$. The normalization condition (2.1) leads to a value of the partition function Z of the form

$$Z(\psi) = \int g(\sigma)\,e^{-\tilde{\beta}\sigma\psi}\mathrm{d}\sigma \tag{2.10}$$

and the locally averaged vorticity (2.2) is expressed as a function of the stream function:

$$\overline{\omega} = -\frac{1}{\tilde{\beta}}\frac{\partial \ln Z}{\partial\psi} = f_{\tilde{\beta},g}(\psi). \tag{2.11}$$

The resulting flow can be calculated by solving the corresponding partial differential equation:

$$-\Delta\psi = f_{\tilde{\beta},g}(\psi) \quad \text{with} \quad \psi = 0 \quad \text{on} \quad (\partial\mathscr{D}). \tag{2.12}$$

A steady Euler flow is characterized in general by the existence of a relationship between vorticity and stream function, so that $f_{\tilde{\beta},g}(\psi)$ selects a particular steady inviscid flow. We notice that in the absence of the energy constraint (i.e $\tilde{\beta} = 0$), the density probability $\rho(\boldsymbol{r},\sigma)$ is uniform so that the mixing is complete. In general, the energy constraint prevents complete mixing and a structure remains. This structure depends on the Lagrange parameters, which are not directly given (we do not know whether their is a thermal bath that could set the temperature of the system, like in standard thermodynamics). The available information is, rather, given as integral quantities, like the energy and the other conserved quantities known from the initial condition. In summary, the stream function ψ is obtained as a function of $\tilde{\beta}$ and $g(\sigma)$ by solving (2.12) and the Lagrange multipliers $\tilde{\beta}$ and $g(\sigma)$ must be related to the conserved quantities thanks to the integral constraints (2.4) and (2.5). In general this procedure yields several solutions for given conserved quantities and the relevant one must have the highest entropy calculated from (2.7) and (2.9).

For any given distribution $\gamma(\sigma)$ of vorticity levels, the accessible energy is restricted between a lower and an upper bound (as discussed and computed by Carnevale & Vallis 1990). Typical behaviour of the equilibrium states in this accessible energy range is represented in figure 1. These states have been numerically computed by Juttner (private communication), using the algorithm of Turkington & Whitaker (1995). Two cases have to be distinguished: with circulation Γ zero or not. When $\Gamma \neq 0$, the entropy versus energy determines a bell-shape curve between these bounds (figure 1*a*). The inverse temperature $\tilde{\beta}$ is the slope $\mathrm{d}S/\mathrm{d}E$ of this curve; it is positive for low energy and negative for high energy. For $\tilde{\beta} > 0$, vorticity is maximum at the domain boundary, while it is rather confined to the central region when $\tilde{\beta} < 0$, as shown in the vorticity fields in figure 1. At the lower and upper energy bounds, any vorticity mixing is forbiden by the energy constraint, and the entropy remains equal to zero. The corresponding slope of the curve S versus E is $\tilde{\beta} = +\infty$ and $\tilde{\beta} = -\infty$ respectively. Between these two bounds, the entropy reaches a maximum with $\tilde{\beta} = 0$, corresponding by contrast to complete mixing, with a uniform coarse-grained vorticity $\Gamma/|\mathscr{D}|$. The flow is then uniquely determined as the solution of the Poisson equation (2.3).

If the circulation Γ is zero, the behaviour at high energy is still similar, as shown in figure 1(*b*). The two vorticity patches, here with values -1 and $+1$, remain unmixed. By contrast the lower energy bound is now zero: the positive and negative vorticity can be arranged into fine intermingled filaments, leading to an arbitrarily small energy as the filament width is decreased. In this limit of small energy, the stream function vanishes, so that the probabilities become uniform, according to (2.9), leading to a maximum entropy at the origin.

In the case of figure 1, the flow topology does not depend on energy, but transitions between different flow structures are often obtained, still with a similar shape for the curve $S(E)$ (see for instance Turkington & Whitaker 1995). These transitions depend on the distribution of vorticity levels, so that general survey of the equilibrim states is a difficult task (even with an efficient numerical method), because of the large number of control parameters. In the present paper, we study the limit of strong mixing, for which the probabilities are close to uniform: this corresponds to an energy range near the maximum of the curve $S(E)$. Then the argument $\tilde{\beta}\sigma\psi$ of the exponential in (2.9)–(2.11) is small and the function $f_{\tilde{\beta},g}(\psi)$ can be linearized. The corresponding entropy, calculated by (3.12) and (3.13), is plotted as dashed lines in figure 1. We observe that the agreement with the exact result is good in a remarkably wide range of energy. This approximation is interesting because a rich bifurcation structure can be studied analytically, providing good insight for the general determination of equilibrium states. Moreover the flow structure depends only on a single control parameter in this limit of strong mixing. Notice also that the relationship $f_{\tilde{\beta},g}$ between vorticity and stream function can be linear even when the linearized approximation is not correct for the entropy. In fact for any energy there exists a particular distribution $\gamma(\sigma)$ of vorticity levels for which $f_{\tilde{\beta},g}$ is linear. It corresponds to a Gaussian $g(\sigma)$ (as noted by Miller, Weichman & Cross 1992). The stream function is then an eigenmode of the Laplacian, and the corresponding probability distribution is given by (2.5) and (2.9).

It will be useful in the following to deal with dimensionless quantities. All the dimensions of the problem can be constructed from a unit of length $|\mathscr{D}|^{1/2}$ and a unit of time $(|\mathscr{D}|/\Gamma_2)^{1/2}$ where $|\mathscr{D}|$ is the area of the domain and Γ_2 the fine-grained enstrophy. This is equivalent to making $|\mathscr{D}| = \Gamma_2 = 1$ and we will take this convention in the following.

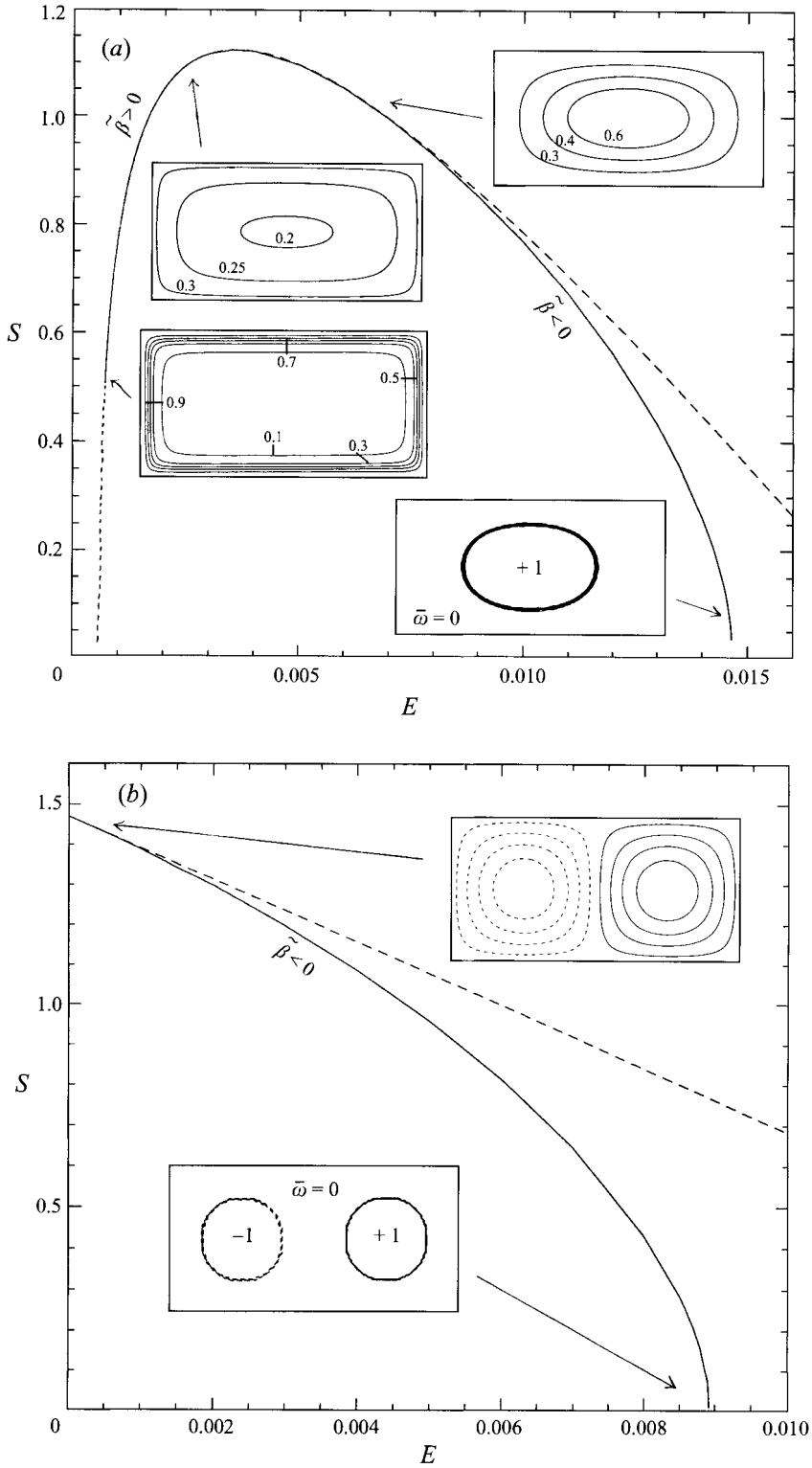

FIGURE 1. For caption see facing page.

2.2. *The limit of strong mixing*

From now on, we shall assume $\tilde{\beta}\sigma\psi \ll 1$ in order to simplify the previous equations. This corresponds to the limit of strong mixing, obtained near the maximum of the curve $S(E)$, as discussed above. It appears in practice that the approximation remains valid even when $\tilde{\beta}\sigma\psi \sim 1$. The relationship $f_{\tilde{\beta},g}$ between vorticity and stream function can be then linearized, so that (2.12) takes the form of a Helmholtz equation:

$$-\Delta\psi + \beta\psi = \beta\langle\psi\rangle + \Gamma, \tag{2.13}$$

$$\psi = 0 \quad \text{on} \quad (\partial\mathscr{D}).$$

The constant on the right-hand side of (2.13) has been written in terms of the domain average $\langle\psi\rangle$ to express the constraint on the total circulation Γ, which must be equal to the domain integral of the vorticity $-\Delta\psi$. The constant β can be determined from the energy constraint (2.4). Expressing the vorticity from the stream function by (2.13) this yields

$$E = \tfrac{1}{2}\beta(\langle\psi\rangle^2 - \langle\psi^2\rangle) + \tfrac{1}{2}\Gamma\langle\psi\rangle. \tag{2.14}$$

The problem (2.13), (2.14) has been obtained at this stage only by assuming a linear relationship between vorticity and stream function, with the constraints of a given circulation Γ and energy E, without specific reference to the statistical theory. Although the partial differential equation (2.13) is linear, the global problem is nonlinear due to the energy constraint (2.14), and it generally exhibits several solutions with bifurcations in the parameter space.

The specific contribution of the statistical theory will be the selection of the solution with the maximum entropy. The statistical theory also specifies the domain of validity of (2.13) as a prediction of the final state resulting from turbulent stirring: this linearized approximation is justified when $\tilde{\beta}\sigma\psi$ is small, as discussed above. A systematic expansion of (2.5) and (2.9)–(2.11) in powers of $\tilde{\beta}\sigma\psi$ is sketched in Appendix A. At first order, it yields (2.13) with the relation

$$\beta = (1 - \Gamma^2)\tilde{\beta}. \tag{2.15}$$

The parameter β is thus the inverse temperature within a multiplicative constant. This constant $1 - \Gamma^2$ is always positive: indeed, due to the Schwartz inequality, $(\int \omega \mathrm{d}^2\boldsymbol{r})^2 \leqslant |\mathscr{D}| \int \omega^2 \mathrm{d}^2\boldsymbol{r}$, so that $\Gamma^2 \leqslant 1$ in non-dimensional form. The expression for the entropy is obtained (see Appendix A) by a corresponding expansion of (2.7) and (2.9), and takes the form $S = S_0 + \mathscr{S}/(1 - \Gamma^2)$, where S_0 is the entropy in the limit of zero energy, for which the probabilities are uniform, $\rho(\boldsymbol{r}, \sigma) = \gamma(\sigma)$, and

$$\mathscr{S} = \tfrac{1}{2}\beta^2(\langle\psi\rangle^2 - \langle\psi^2\rangle) \tag{2.16}$$

Notice that according to (2.13), (2.14), and (2.16), the only conserved quantities that we have to take into account in the limit of strong mixing are the energy E and the circulation Γ. Moreover, it will appear that the *structure* of the equilibrium state

---

FIGURE 1. Entropy versus energy for a given distribution of probability levels, in the rectangular domain 2×1. The initial condition is (*a*) a patch of vorticity $+1$ and area $1/2$ corresponding to a circulation $\Gamma = 0.5$, or (*b*) two patches with values $+1$ and -1 and the same area $1/4$, corresponding to a circulation $\Gamma = 0$. The long-dashed lines correspond to the prediction $S(E)$ given by (3.13) and (3.12) in the limit of strong mixing. The associated vorticity fields are indicated by isocontour plots (the numerical computations have been provided by B. Juttner, using the algorithm of Turkington & Whitaker 1995. The short-dashed line corresponds to the limit of convergence of the computation).

depends only on a *single control parameter* Λ whose expression is

$$\Lambda = \frac{\Gamma}{(2E)^{1/2}}. \tag{2.17}$$

In fact, the structure depends only on Λ^2: the solution associated with a negative Λ can be obtained from the solution corresponding to $-\Lambda \geqslant 0$ by simply reversing the signs of the vorticity and the stream function.

3. General form of the solutions for an arbitrary domain

In this section the domain $(\mathscr{D})$ is somewhat arbitrary but must not possess any specific continuous symmetry that would induce new conserved quantities. In the limit of strong mixing, the stream function satisfies the Helmholtz equation (2.13). Two cases have to be taken into account depending on whether ψ is or is not an eigenmode of the Laplacian.

3.1. *Eigenmode solutions*

As a first case, we assume

$$\beta\langle\psi\rangle + \Gamma = 0 \tag{3.1}$$

so that ψ is an eigenmode ψ_n of the Laplacian in the domain $(\mathscr{D})$, and $\beta = \beta_n$ is the corresponding eigenvalue. The inverse temperature β_n is then necessarily negative (since $2E = -\int \psi_n(\beta_n\psi_n)\mathrm{d}^2\boldsymbol{r} > 0$). More precisely, according to (2.14) and (3.1) we can write the stream function in the form

$$\psi = \pm\left(\frac{2E}{-\beta_n}\right)^{1/2}\psi_n \tag{3.2}$$

where we have introduced the orthonormal set $\{\psi_n\}$ ($\langle\psi_n{}^2\rangle = 1$) of eigenmodes for the Laplacian that vanish on $(\partial\mathscr{D})$. These solutions (3.2) exist only for discrete values Λ_n of the control parameter Λ, that can be computed from (2.17), (3.1) and (3.2):

$$\Lambda_n^2 = -\beta_n\langle\psi_n\rangle^2. \tag{3.3}$$

This equation displays two types of eigenmodes denoted by primes and double primes respectively: those with a zero mean value $\langle\psi_n'\rangle = 0$ that can exist for $\Lambda = 0$ only; and those with a non-zero mean value $\langle\psi_n''\rangle \neq 0$ that exist for $\Lambda = \Lambda_n'' \neq 0$, given by (3.3) (see figure 2, discrete modes).

3.2. *The solutions of the continuum*

We now consider the case where $\beta\langle\psi\rangle + \Gamma \neq 0$. We can then eliminate the spatial average in (2.13) by introducing the reduced solution $\phi_\beta = \psi/(\beta\langle\psi\rangle + \Gamma)$, or equivalently

$$\psi = \frac{\Gamma\phi_\beta}{1 - \beta\langle\phi_\beta\rangle} \tag{3.4}$$

where ϕ_β is the function satisfying

$$-\Delta\phi_\beta + \beta\phi_\beta = 1, \tag{3.5}$$

$$\phi_\beta = 0 \quad \text{on} \quad (\partial\mathscr{D}).$$

This equation indeed admits a single solution provided β is not an eigenvalue β_n of the Laplacian (the case $\beta = \beta_n$ will be considered in the next sub-section). If we

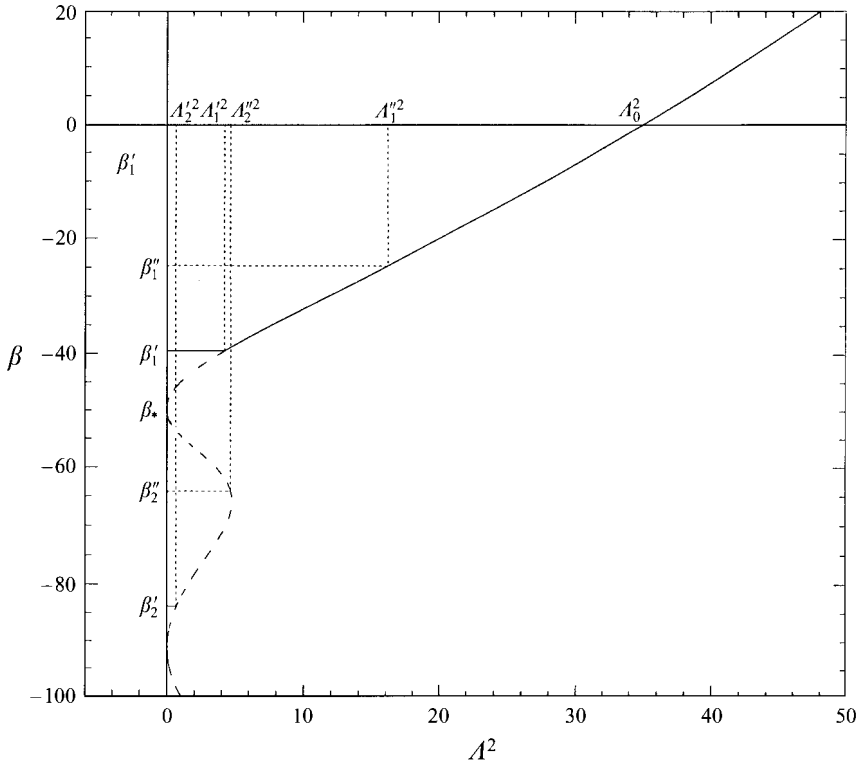

FIGURE 2. Relationship between A^2 and β given by (3.7) (for a rectangular domain with aspect ratio 2). The horizontal plateaux corresponding to the 'mixed solutions' at $\beta = \beta_1', \beta_2' \ldots$ are also represented. The two kinds of eigenvalues, and the corresponding values of A^2 are indicated. The dashed part of the line corresponds to solutions of (2.13) with $\beta < \beta_1'$, and are not local entropy maxima.

expand ϕ_β over the set of eigenmodes ψ_n and substitute in (3.5), we find

$$\phi_\beta = \sum_m \frac{\langle \psi_m'' \rangle}{\beta - \beta_m''} \psi_m'' \tag{3.6}$$

involving only the eigenmodes ψ_m'' with non-zero average (the other eigenmodes are not 'excited' by the second term in (3.5)).

The inverse temperature β is implicitly determined, as a function of the conserved quantities, by the energy constraint (2.14). It will be convenient to write this constraint in the form (see Appendix B)

$$F^2(\beta) = A^2 F'(\beta) \tag{3.7}$$

where we have introduced the function

$$F(\beta) \equiv \beta \langle \phi_\beta \rangle - 1 \tag{3.8}$$

The equation of state (3.7) determines A^2 as a function of β, as represented in figure 2. We need to invert this function, determining a set of possibles values of β from the control parameter A^2. Figure 2 has been numerically obtained in a rectangle with aspect ratio 2, but the shape of the curve A^2 versus β is quite general, and can be understood by the mathematical properties of the function F, as derived in

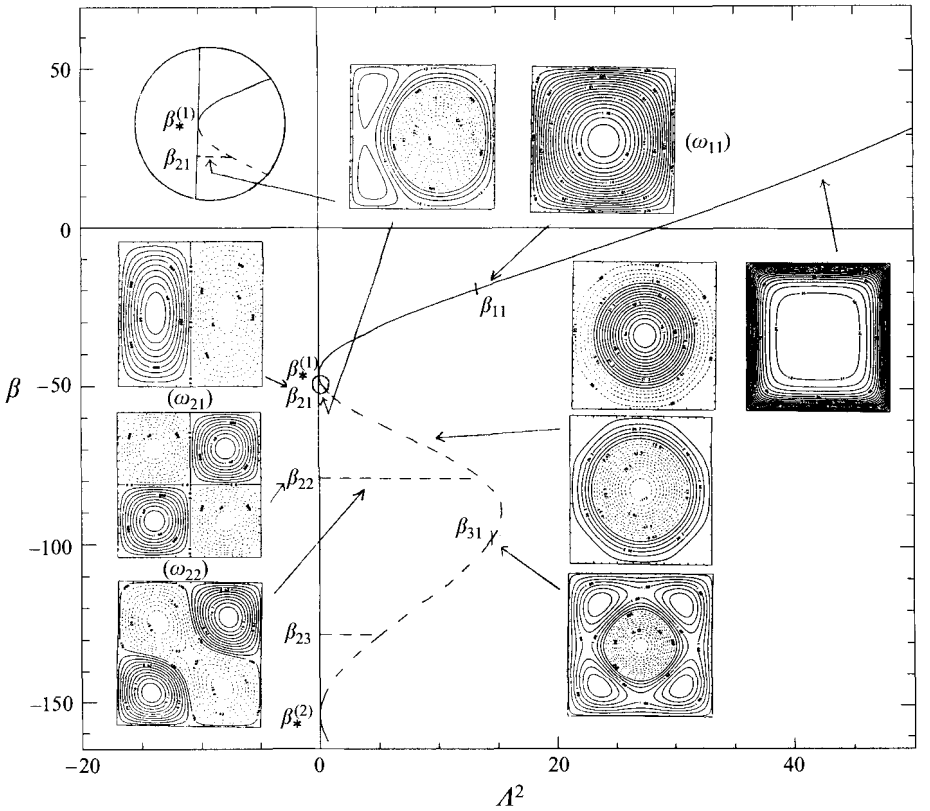

FIGURE 3. Vorticity iso-lines for solutions of (2.13) in the square domain, corresponding to the different parts of the $\Lambda^2 - \beta$ diagram (analogous to figure 2) ($\omega > 0$ as solid lines, $\omega < 0$ as dashed lines).

Appendix C. The case of a square is for instance shown in figure 3, together with representative vorticity fields.

For small Λ^2, a pair of solutions is found around each zero $\beta = \beta_*^{(n)}$ of the function $F(\beta)$. We can then expand F around $\beta \sim \beta_*^{(n)}$, so that (3.7) yields

$$\beta = \beta_*^{(n)} \pm \kappa_{(n)} \left(\Lambda^2\right)^{1/2} \tag{3.9}$$

where $\kappa_{(n)} = 1/F'(\beta_*^{(n)})^{1/2}$. These multiple solutions must be classified according to their entropy, and compared to the 'mixed solutions' (see §§3.3 and 3.4).

By contrast, for high values of Λ^2, equation (3.7) yields only one solution. When $\Lambda^2 = \Lambda_0^2$, we have $\beta = 0$ so that the vorticity is uniform in the whole domain (complete mixing). When $\Lambda^2 \leqslant \Lambda_0^2$ (negative temperatures) the vorticity has a tendency to fill the core of the domain and form structures but when $\Lambda^2 \geqslant \Lambda_0^2$ (positive temperatures) it instead concentrates near the boundaries. This increase of the parameter Λ^2 is obtained for instance when we increase the circulation Γ for a fixed (small) energy. We then describe a continuous change of behaviour from figure 1(*a*) to figure 1(*b*), near the origin (low energy): the slope β is negative for small circulation and becomes positive for larger circulations (the linear approximation however remains valid for large Λ^2 only when $\Gamma^3/E \ll 1$, see Appendix C, and is not satisfied when approaching the low-energy bound of curve A, with unmixed vorticity).

3.3. *Mixed solutions; analogy with phase transitions*

In the last subsection, we have discussed the case when β is not an eigenvalue of the Laplacian, so that (3.5) has a unique solution (for a given β). When β tends to an eigenvalue β_n'' of the Laplacian (such that $\langle\psi_n''\rangle \neq 0$), then ϕ_β diverges and is dominated by the single term proportional to ψ_n'' in (3.6). The corresponding state ψ, given by (3.4), then smoothly tends to the eigenmode solution (3.2). By contrast, if $\beta = \beta_n'$ (i.e. with $\langle\psi_n'\rangle = 0$), (3.5) has still the solution (3.6), but it is not unique: a new solution is obtained by adding the eigenmode ψ_n'. The general solution of (3.5) is then the linear combination of:

$$\phi_{\beta_n'} = \sum_m \frac{\langle\psi_m''\rangle}{\beta_n' - \beta_m''}\psi_m'' + c_n\psi_n'. \tag{3.10}$$

These solutions correspond to the 'plateaux' at $\beta = \beta_1'$ and $\beta = \beta_2'$ represented in figures 2 and 3. The constant c_n can be computed as a function of A^2 from the energy constraint (2.14), and the stream function ψ is still given by (3.4). Two special limits are worth noticing: for $A = 0$ we recover the pure eigenmode (3.2) ($c_n \to \infty$), while we have $c_n = 0$ and recover (3.6) for $A = A_n'$, defined by introducing $\beta = \beta_n'$ in (3.7). These limits correspond to the two ends of the plateaux shown in figure 2.

These mixed solutions can be physically interpreted as the coexistence of two thermodynamic phases. Solution (3.4) can be said to form a continuous phase, for which (3.7) can be interpreted as an equation of state, while solution (3.2) forms a phase only defined for discrete (inverse) temperatures β_n'. The coexistence of these two phases is possible for $\beta = \beta_n'$ only, like the coexistence of a liquid and a solid phase at the transition temperature. The proportion of the two phases, corresponding to the coefficient c_n, is then determined by the energy. This is the sum of the energy of each phase, because of the orthogonality of the function ψ_n' with the other eigenmodes used in the expansion (3.6).

3.4. *Selection of the solutions by their entropy*

We have obtained several solutions for a given value of the control parameter A. A choice can be made by comparing their entropy and selecting the solution with the highest value. Notice that a solution with a lower entropy may still be relevant as a metastable state, and this has to be settled by determining whether it is a local entropy maximum. This question will be considered in the next subsection, and we here only compare the entropy of the different solutions, computed from (2.16).

In the case of the eigenmode solutions (3.2), the entropy of mode n is

$$\mathscr{S}_n = \beta_n E\left(1 + \frac{A_n^2}{\beta_n}\right). \tag{3.11}$$

In the case of eigenmodes with zero net circulation, the entropy reduces to

$$\mathscr{S}_n = \beta_n E. \tag{3.12}$$

This proves on the grounds of the statistical theory that the mode with the highest entropy is the fundamental ($n = 1$).

However this has to be compared with the entropy of the solutions in the continuum. The expression for the entropy (2.16) then yields

$$\mathscr{S} = \beta E\left(1 + A^2\frac{1 + F(\beta)}{\beta F(\beta)}\right). \tag{3.13}$$

For $A = 0$, we have simply $S = \beta_*^{(n)} E$, so that the first root $\beta_*^{(1)}$ of the function F has the maximum entropy in the continuum. The comparison with the first eigenmode solution with zero average will depend on the respective positions of $\beta_*^{(1)}$ and the eigenvalue β_1'. This depends on the shape of the boundary as shown in the case of a rectangular domain with different aspect ratios (see §4): in the square, $\beta_*^{(1)} > \beta_1'$, so that the continuum solution is selected, but the contrary is obtained for a rectangle with aspect ratio greater than 1.12.

For A^2 small, we can expand (3.13) around $\beta = \beta_*^{(1)}$, using the approximation (3.9), which yields

$$\mathscr{S} = \left(\beta_*^{(1)} \pm 2\kappa_{(1)} A\right) E. \tag{3.14}$$

The solution with the highest β has the highest entropy, as expected. This solution is in competition with the mixed state, whose entropy is still given by (3.13), and the selection will depend on the respective positions of $\beta_*^{(1)}$ and β_1', in continuity with the case $A = 0$.

3.5. *Second-order variations*

The previous solutions cancel the first constrained variations of the entropy (they are critical points), but are not necessarily maxima. To settle this, we have to check whether the second-order variations $\delta^2 S < 0$ for any variation that *strictly* conserves the constraints. This is equivalent to checking that the second variations of the functional (free energy)

$$J = S - \tilde{\beta} E - \int \tilde{\alpha}(\sigma)\gamma(\sigma)\mathrm{d}\sigma - \int \tilde{\zeta}(\boldsymbol{r})\left(\int \rho(\boldsymbol{r},\sigma)\mathrm{d}\sigma\right)\mathrm{d}^2\boldsymbol{r} \tag{3.15}$$

are strictly negative for any small variation $\delta\rho(\boldsymbol{r},\sigma)$ which does not change the constraints *at first order*. A Taylor expansion of the general expressions for the energy (2.4) and entropy (2.7) yields

$$\delta^2 J = -\frac{1}{2}\int \frac{(\delta\rho)^2}{\rho}\mathrm{d}^2\boldsymbol{r}\mathrm{d}\sigma - \frac{1}{2}\tilde{\beta}\int \delta\psi\delta\overline{\omega}\mathrm{d}^2\boldsymbol{r} \tag{3.16}$$

(the second variations of the other constraints vanish). The integral of the second term can be written $\int(\nabla\delta\psi)^2\mathrm{d}^2\boldsymbol{r}$ which is always positive. Therefore, when $\tilde{\beta}$ is positive, $\delta^2 J$ is negative and the (single) critical point is a maximum. It is still a maximum as long as $\tilde{\beta}$ is greater than the first eigenvalue of the Laplacian, β_1'', as stated by Robert & Sommeria (1991). For smaller values of $\tilde{\beta}$, the selection of entropy maxima is not given by any simple criteriom.

However in the limit of strong mixing, it is possible to discard some solutions of (2.13) as non-maxima, when β is smaller than β_1'. For that purpose we consider a particular variation of the form

$$\delta\rho(\boldsymbol{r},\sigma) = \gamma(\sigma)(\sigma - \Gamma)\psi_1'(\boldsymbol{r}). \tag{3.17}$$

This perturbation is in a mode with zero mean, so it does not change the circulation; and the dependency in σ has been set to keep the normalization condition (2.1) unchanged. The basic state is assumed to be a solution of the continuum, or an eigenmode of the Laplacian with $\beta_n < \beta' 1$, so that the perturbation is orthogonal to this basic state. Therefore neither the energy constraint, nor all the other constraints, are modified at first order by the perturbation (3.17). In the limit of strong mixing, we

can make the approximation $\rho(\boldsymbol{r},\sigma) \simeq \gamma(\sigma)$ in the first integral of (3.16), and obtain

$$\delta^2 J = \frac{1}{2}(1-\Gamma^2)\left(\frac{\beta}{\beta_1'}-1\right) \tag{3.18}$$

which is strictly positive when $\beta < \beta_1'$. It follows that for $\beta < \beta_1'$, the critical point cannot be a local maximum for the entropy. Thus, every solution beneath the 'plateau' $\beta = \beta_1'$ in figure 2 is not only a state with a lower entropy than the corresponding mixed mode (for a given A): it is *not even a local maximum.* In physical terms, it can be destabilized by a perturbation ψ_1' (the first eigenmode with a zero net circulation). Since $\beta \sim 1/\ell^2$, where ℓ is the typical scale of the flow, this result corresponds to the observation that vortices tend to merge to form structures with larger scales, which increases the entropy for given integral constraints.

In the case $\beta_1' < \beta_*^{(1)}$, the corresponding eigenmode ψ_1' has a lower entropy than the continuum, and we now show moreover that it is *not even a local entropy maximum.* We use a similar method, applying to ψ_1' a particular variation of the form

$$\delta\rho(\boldsymbol{r},\sigma) = \gamma(\sigma)(\sigma-\Gamma)\left(1-\beta_*^{(1)}\phi_{\beta_*^{(1)}}(\boldsymbol{r})\right) \tag{3.19}$$

constructed from the mode of the continuum with zero circulation. As before, this perturbation changes neither the circulation nor the normalization condition. Moreover its Fourier decomposition (3.6) does not involve eigenmodes with zero circulation, so that it is orthogonal with the basic state ψ_1', and does not change the energy at first order. As previously, we calculate the second variation of the free energy:

$$\delta^2 J = \tfrac{1}{2}(1-\Gamma^2)\,F'(\beta_*^{(1)})(\beta_*^{(1)}-\beta_1') \tag{3.20}$$

which is strictly positive if $\beta_*^{(1)} > \beta_1'$ (since $F' > 0$, see Appendix C). Therefore when $\beta_1' < \beta_*^{(1)}$, the eigenmode solution ψ_1' is not a local entropy maximum (it can be destabilized by a perturbation with the structure of the first solution of the continuum with zero mean). The solutions of the continuum at the other end of the plateau (i.e. for $\beta < \beta_1'$) are also not maxima (as shown above), so we expect that this property persists by continuity along the whole plateau, since no other branch of solutions is crossed.

4. Application to a rectangular domain

4.1. *Predictions in the limit of strong mixing*

We now illustrate these general results for the case of a rectangular domain whose sides are denoted by $a = \tau^{1/2}$ and $b = 1/\tau^{1/2}$ (where $\tau = a/b \geqslant 1$ is the aspect ratio). For this domain, the eigenmodes and the corresponding normalized eigenfunctions are explicitly given by

$$\beta_{nm} = -\left(\frac{n^2}{\tau}+\tau m^2\right)\pi^2. \tag{4.1}$$

$$\psi_{nm} = 2\sin(n\pi x/\tau^{1/2})\sin(m\pi\tau^{1/2}y) \tag{4.2}$$

(where the origin of the Cartesian frame is taken at the lower left corner of the domain). The integer $n \geqslant 1$ gives the number of vortices along the x-axis while $m \geqslant 1$ gives the number of vortices along the y-axis. We can check that $\langle\psi_{nm}\rangle = 0$ if n or m

is even and $\langle \psi_{nm} \rangle = 8/(nm\pi^2)$ if n and m are odd. The eigenvalues defined in §3 can now be explicitly given. For example, we have

$$\beta_1'' = \beta_{11} = -\left(\frac{1}{\tau} + \tau\right)\pi^2, \tag{4.3}$$

$$\beta_1' = \beta_{21} = -\left(\frac{4}{\tau} + \tau\right)\pi^2. \tag{4.4}$$

The solutions for the continuum are obtained by a numerical resolution of the Helmholtz equation (3.5) for a set of parameters β. We then tabulate the functions $F(\beta)$ and $F'(\beta)$, determined from the computed stream function by (3.8), (B2.4), and plot β versus A^2. This curve is indicated in figure 3 for the case of a square domain ($\tau = 1$); it is quite similar to the case of a rectangle with $\tau = 2$, plotted in figure 2, in agreement with the general properties derived in Appendix C. We have also represented in figure 3 the vorticity fields corresponding to different points along the curve β versus A^2. The stream lines of the continuum preserve the symmetries of the domain (since the solution ϕ_β of (3.5) is unique for a given β), with an extremum at the box centre. Secondary vorticity extrema appear for low (negative) values of β (as the 'mark' of the eigenmodes of higher order encountered along the continuum), but these solutions are not relevant, as they are not local entropy maxima for $\beta < \beta_{21}$ (see §3.5). Therefore the solutions of the continuum will be called *monopoles*.

The mixed solutions involving the eigenmodes with zero mean are also plotted in figure 3, and correspond to the horizontal lines on the graph β versus A^2. These lines start with the pure eigenmode at $A^2 = 0$ and join the continuum smoothly, as $c_n \to 0$ in (3.10). The mixed solutions involving the modes higher than (2, 1) are not local entropy maxima and must be eliminated (at least in the limit of strong mixing), like the mode (2, 2) represented in figure 3. Therefore the relevant mixed solutions involve only the *dipole* structure.

The competition between the monopole and dipole solutions is settled by comparing their entropy for a given value of the control parameter A. The entropy of the different branches is calculated by (3.11), (3.13) and plotted in figure 4 for the case of the square. We observe that the monopole always has the highest entropy and is therefore predicted for any value of A, while the dipole is not even a metastable state, as shown in §3.5. In the monopoles with small $A > 0$, the positive vorticity gathers in the central region, while the negative vorticity remains on the periphery. The reversed monopole, with negative vorticity at the centre, is also a solution, but it has a lower entropy (corresponding to the dashed line in figure 4). These two configurations become equivalent at $A = 0$, where the two branches join, but remain quite distinct physical states (with opposite velocity). This corresponds to a parity breaking for the final organization of the system: the flow spontaneously rotates in either direction, although it has a zero circulation. For a weak non-zero circulation (A small), the reversed monopole is probably still a local entropy maximum by continuity. In any case, it is not even a local maximum beyond the junction with the branch $\beta = \beta_{21}$ (point M in figure 4), as stated in §3.5.

In the case of a rectangle with sufficiently large aspect ratio τ, the dipole has a higher entropy than the monopole, in contrast to the square. The dipole mixed state is then predicted along the branch $\beta = \beta_{21}$, as shown in figure 5. The competition between the monopole and dipole for weak circulation is settled by the comparison of β_{21} and $\beta_*^{(1)}$, the first zero of the function F. These two numbers, proportional to the entropy of each solution for $A = 0$, by (3.12) and (3.14), are plotted versus the

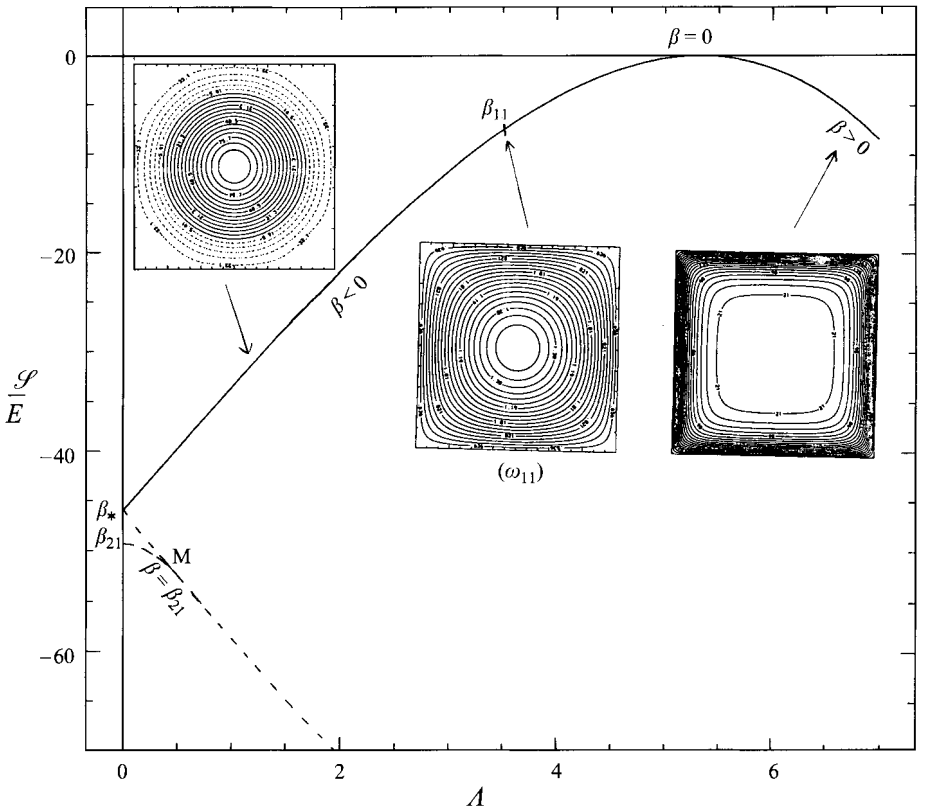

FIGURE 4. Entropy of the main modes in the square domain versus the control parameter Λ. The solution with the highest entropy is along the solid line, and the others are along the dashed lines. The solution of the continuum (monopole) always has the highest entropy. For negative β (and $\Lambda > 0$), the vorticity is maximum at the centre, and negative vorticity is pushed toward the edge, while for positive β the vorticity is maximum on the edge (and vorticity is uniform for $\beta = 0$). The dipolar solution (branch $\beta = \beta_{21} = -49.35$) has a lower entropy, as does the reversed monopole, along the dashed lines. More precisely, we have shown in §3.5 that neither the dipole (since $\beta_{21} < \beta_*^1 = -46.1$) nor the solutions below point M are local entropy maxima.

aspect ratio τ in figure 6. We clearly see the crossover at $\tau \simeq 1.12$, beyond which the dipole dominates.

4.2. *Validation and discussion*

As a simple example of an application, consider an initial state with zero circulation ($\Gamma = 0$) in the square domain with area unity. We then predict a final organization into a monopole (figure 4), with $\beta = \beta_*^{(1)} \simeq -46.1$. The actual stream function ψ is obtained from ϕ_β by (3.4), but the expression is undetermined for $\Gamma = 0$ (then $\beta\langle\phi_\beta\rangle - 1 \equiv F(\beta) = 0$ from (3.7)). We have therefore rather to take the limit $\Lambda \to 0$ in (3.4), using (2.17) and (3.7)–(3.8), which yields

$$\psi(x,y) = \pm\left(\frac{2E}{F'(\beta_*^{(1)})}\right)^{1/2} \phi_{\beta_*^{(1)}}(x,y). \tag{4.5}$$

The arbitrary sign corresponds to the two possible directions of spontaneous rotation as discussed in §4.1. We numerically obtain $F'(\beta_*^{(1)}) \simeq 2.44 \times 10^{-2}$ and a maximum 7.88×10^{-2} for $|\phi_{\beta_*^{(1)}}|$ (reached at the box centre).

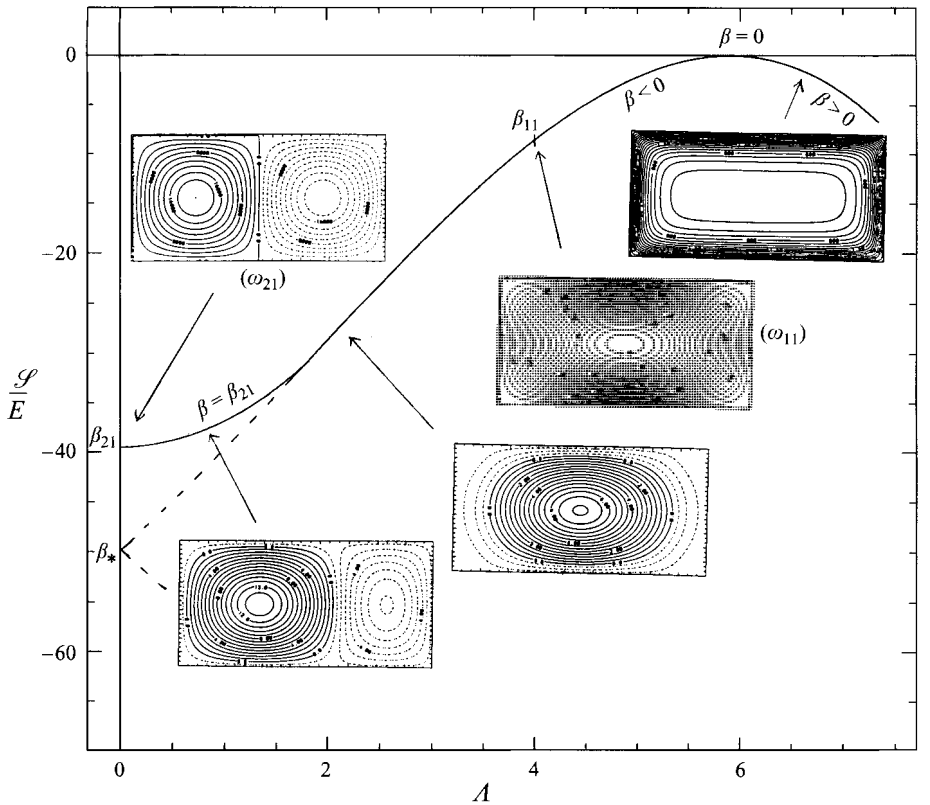

FIGURE 5. Same as figure 4, but for the rectangular domain with aspect ratio 2. The mixed solution now has the highest entropy along the line $\beta = \beta_{21} = -39.5 > \beta_*^{(1)} = -50$, and joins continuously the monopole solution for $A = A'_{21} = 2.06$.

We can then estimate the quality of the linearized approximation by calculating the higher-order terms in (A11). They increase with the typical magnitude of ψ, depending on the energy E by (4.5). The nonlinear correction depends on the moments Γ_3 and Γ_4 of the initial vorticity field. In the case of a symmetrical initial vorticity distribution, $\Gamma_3 = \Gamma_1 = 0$, it depends only on the kurtosis $Ku = \Gamma_4/\Gamma_2^2$. The correction is proportional to $Ku - 3$, so that we expect that the linearized approximation remains particularly good, even at fairly high energy, when the kurtosis is equal to 3, for instance with a Gaussian distribution (see the end of §2.1).

Let us consider the simple example of four alternating vortices in the square domain with side unity, represented by the stream function $\psi_0(x, y) = (1/4\pi^2) \sin 2\pi x \sin 2\pi y$ (normalized such that $\Gamma_2 = 1$). The corresponding probability distribution of vorticity $\gamma(\sigma)$ is a bell-shape symmetric curve, maximum at $\sigma = 0$, and vanishing beyond the vorticity extrema $\sigma = \pm 2$. The energy is $E = 1/16\pi^2$, which sets the maximum stream function $\psi_{max} = 4.0 \times 10^{-2}$ by (4.5) and the numerical values given above (we assume that the system organizes with a positive $\langle\psi\rangle$, but the other sign would be equivalent). The maximum value of the argument in (2.9), reached for $\sigma = 2$ and $\psi = \psi_{max}$, is $\beta\sigma\psi = 3.7$, which is not small. However this is only an extreme value, with little effect on the locally averaged vorticity field. The nonlinear correction to the curve $\omega - \psi$ is better estimated by (A11). We have $\beta\langle\phi_\beta\rangle \equiv 1 + F(\beta) = 1$, since $F(\beta) = 0$ for $\beta = \beta_*^{(1)}$, so that $\beta < \psi >= -0.509$, using (4.5). From the initial

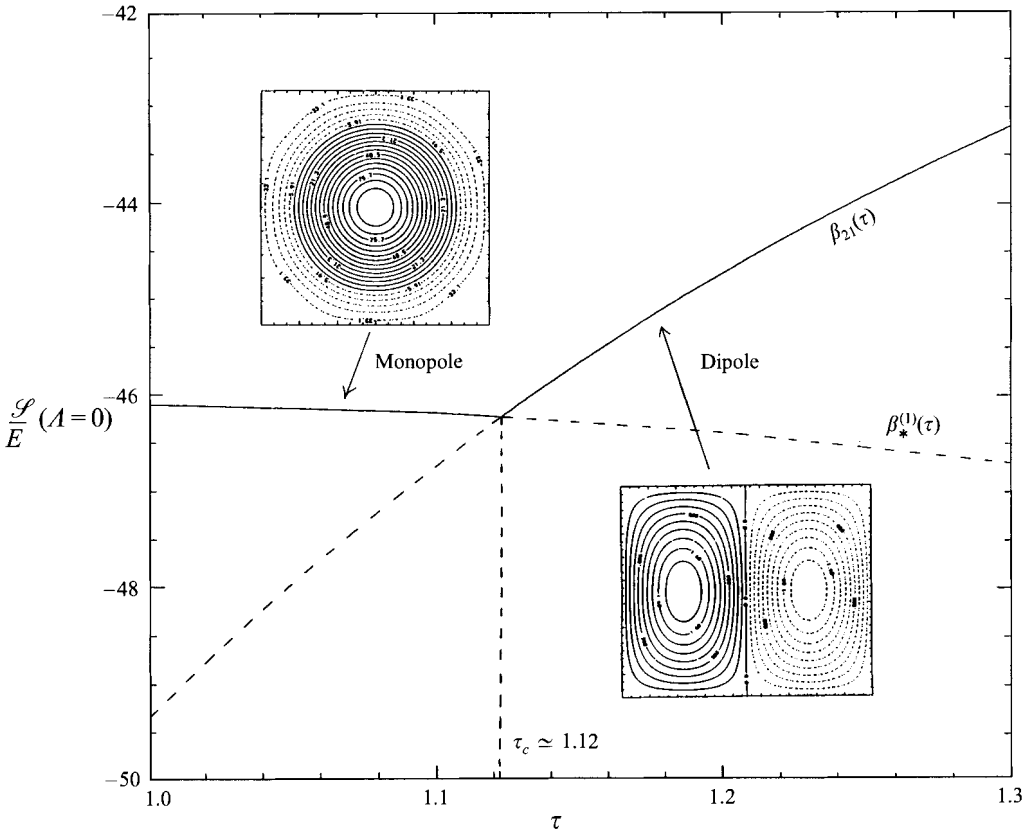

FIGURE 6. Entropy of the monopole and the dipole in a rectangular domain versus the aspect ratio τ. The selected structure is the monopole when $\tau < 1.12$, and the dipole when $\tau > 1.12$.

condition we calculate $Ku - 3 = -3/4$. The resulting values for the coefficients in (A11) are $B_2 = 0.191\ \beta^2$ and $B_3 = 0.125\ \beta^3$, and the maximum values for the nonlinear corrections $B_2\psi_{max}^2 = 0.65$ and $B_3\psi_{max}^3 = -0.79$. The resulting correction (-0.14) is smaller than the linear term $B_1\psi_{max} \sim -\beta\psi_{max} = 1.85$ (it would have to be corrected by the actual perturbative resolution of (A11) with the integral constraints). Therefore the linear approximation is a reasonable first approach in this case.

The numerical solution of the maximization problem, solving the nonlinear equation (2.12), has been obtained by Juttner *et al.* (1995) for an initial condition with zero circulation in a square. The solution then depends on the initial distribution of the vorticity levels, and a choice of patches with positive and negative vorticity is made. An organization into a monopole is obtained at moderate energy, in agreement with our result. A similar organization has also been obtained by Pointin & Lundgren (1976) with point vortex statistics, corresponding to a limit of small-area vortices. Our analysis, although providing less precise predictions, yields a wider understanding of these results, and allow one to classify them in more general cases. Qualitative discrepency with our results appears only for fairly peculiar initial conditions, close to the energy upper bound. A dipolar state is then obtained by Juttner *et al.* (1995), with two possible orientations depending on the initial vorticity area.

These predictions are also found to be in good agreement with a variety of numerical simulations and laboratory experiments (Juttner *et al.* 1995; Verron & Sommeria 1987; Marteau, Cardoso & Tabeling 1995). For a four-vortex initial

condition, as we have considered here, two vortices of the same sign are observed to merge, while the two vortices of the opposite sign are stretched around, leading to the predicted monopole final state. By contrast, numerical simulations indicate organization into a dipolar state for a rectangle with aspect ratio 2 (Juttner, private communication). Numerical simulations of Montgomery & Joyce (1974), using a point vortex dynamical code, and laboratory experiments of spin-down (van Heijst, Davies & Davis 1990) also show organization into a dipolar state for a rectangular domain. However a more precise test of the predicted transition with aspect ratio should be undertaken.

When the initial condition is at smaller scale, involving a pattern with more than four vortices, the energy (normalized by the enstrophy) is smaller, so that our linear approximation is still better justified in principle. An organization into a global rotation has been for instance obtained for two-dimensional turbulence forced at small scale in a square box (Sommeria 1986). Occasional reversals of the rotation have been observed in this laboratory experiment, interpreted as a switching between the two stable states, under random turbulent fluctuations. We now provide a clear explanation of this behaviour in terms of statistical mechanics. By contrast, in a laboratory experiment of freely decaying two-dimensional turbulence, Marteau *et al.* (1995) obtain a dipolar final state for an initial condition at small scale, and the $\omega - \psi$ relationship displays a significant concave shape. This is still consistent with the statistical theory, but corresponds to a case of high energy and low vorticity area (therefore high kurtosis), rather than the integral constraints expected from the initial condition. A similar conclusion is obtained from typical numerical computations of two-dimensional turbulence, initiated at small scale in a doubly periodic domain. The final $\omega - \psi$ relationship is then close to a sinh curve, as analysed by Montgomery *et al.* (1992). Yet the initial condition corresponds to a low energy, for which our linearized analysis is quite justified (and would simply yield the fundamental sine-shape eigenmode in the doubly periodic case). We can interpret this discrepency by considering that the evolution is then long, involving successive vortex mergings, and the probability distribution of vorticity changes under viscous effects: enstrophy is dissipated and vorticity remains concentrated in small vortex cores. The effective initial condition to consider is the vorticity distribution just before the last merging event leading to the global self-organization: the energy normalized by enstrophy is high (since enstrophy has decreased with constant energy), the area of non-zero vorticity is small, and the observed shape of $f_{\beta,g}$ is then in agreement with theory. Of course its predictive power is then limited, as long as a correct treatment of viscous effects is not given.

5. Circular domain

The domain ($\mathscr{D}$) is now a disk of radius $a = 1/\pi^{1/2}$. We have a new conserved quantity (resulting from the rotational symmetry) that is the angular momentum:

$$L = \int \overline{\omega} r^2 \mathrm{d}^2 \boldsymbol{r}. \tag{5.1}$$

It can be taken into account in the variational principle (2.8) by adding a new Lagrange multiplier denoted $\tilde{\beta}\Omega/2$. Then the optimal density probability becomes

$$\rho(\boldsymbol{r}, \sigma) = \frac{1}{Z} g(\sigma) \mathrm{e}^{-\tilde{\beta}\sigma(\psi + \Omega r^2/2)} \tag{5.2}$$

and the relation between the locally averaged vorticity and the stream function takes the form $\overline{\omega} = f_{\tilde{\beta},g}(\psi + \frac{1}{2}\Omega r^2)$ where $f_{\tilde{\beta},g}$ is given by (2.11). This relation defines either an axisymmetric flow, or a set of symmetry-breaking flows differing by their angular phase. Such a set of solutions appears from the statistical theory as the most probable outcome of a random selection from microscopic states (with the appropriate integral constraints). However, it is remarkable that such a set of equivalent equilibria corresponds in fact to the same solution of the Euler equation steadily rotating with angular velocity Ω. Then, it is natural to introduce the relative stream function ψ' defined by

$$\psi(r, \theta, t) = \psi'(r, \theta - \Omega t) - \frac{\Omega}{2}\left(r^2 - \frac{1}{\pi}\right) \tag{5.3}$$

and the corresponding vorticity $\overline{\omega}' = -\Delta\psi'$. Using (5.3) we get

$$\overline{\omega} = \overline{\omega}' + 2\Omega \quad \text{and} \quad \Gamma = \Gamma' + 2\Omega \tag{5.4}$$

where quantities with primes describe the fluid in the rotating frame ($\mathscr{R}'$) in which the equilibrium flow is stationary: indeed in this new frame, the vorticity $\overline{\omega}'$ is a function of ψ' alone.

We now assume that this function can be linearized, leading to an equation with the same form as (2.13):

$$\Delta\psi' + k^2\psi' = k^2\langle\psi'\rangle - \Gamma', \tag{5.5}$$

$$\psi' = 0 \quad \text{on} \quad (\partial\mathscr{D})$$

where we assume a negative coefficient $\beta \equiv -k^2 \leqslant 0$ (we shall see below how to extend the results for a positive coefficient). The parameter k^2 and the angular velocity Ω are determined from the conserved quantities in the initial frame of reference, leading to the following constraints, obtained by combining (2.4) (5.1) and (5.5):

$$L = k^2\left(\langle\psi' r^2\rangle - \frac{\langle\psi'\rangle}{2\pi}\right) + \frac{\Gamma}{2\pi}, \tag{5.6}$$

$$E = \tfrac{1}{2}k^2(\langle\psi'^2\rangle - \langle\psi'\rangle^2) + \tfrac{1}{2}\Gamma\langle\psi'\rangle - \tfrac{1}{4}\Omega L + \frac{\Omega\Gamma}{4\pi}. \tag{5.7}$$

Like in §2.2, we can justify the linearized equation (5.5) as an expansion of the equilibrium state in terms of the small quantity $\tilde{\beta}\sigma\psi' \ll 1$, in the limit of strong mixing. This yields the relation analogous to (2.15):

$$\beta = -k^2 = (1 - \Gamma^2)\tilde{\beta}.$$

The entropy is given by (2.16) with the substitution $\psi \to \psi'$:

$$\mathscr{S} = \tfrac{1}{2}\beta^2(\langle\psi'\rangle^2 - \langle\psi'^2\rangle). \tag{5.8}$$

The study is then very similar to the previous one, but the main difference is that we have to deal with two integral constraints (5.6) and (5.7) instead of one. It will appear that the flow *structure* still depends only on a single control parameter A given by

$$A = \left(\frac{3\pi}{4H}\right)^{1/2}\left(\frac{\Gamma}{2\pi} - L\right) \tag{5.9}$$

with

$$H = E + \frac{\Gamma L}{4} - \frac{3\Gamma^2}{16\pi} \tag{5.10}$$

(we can show that $H \geqslant 0$, see Appendix B). The equilibrium flow is fully determined

by the three initial parameters Γ, L and E. These various initial conditions yield the same flow structure for a given value of A, but with different rotation rate Ω and energy E.

In the case of a circular domain, the Helmholtz equation can be explicitely solved in terms of Bessel functions. We can recover the three kinds of solutions that we have studied in §3.

(i) The eigenfunctions with a vanishing mean value are given by

$$\psi' = CJ_n(kr)\sin(n\theta + \delta) \tag{5.11}$$

with $n \neq 0$, where J_n is the Bessel function of the first kind with order n. Their angular average at each radius vanishes, so that from (5.6), these solutions are only obtained for $A = 0$. Their relative circulation Γ' vanishes, so that the angular velocity is $\Omega = \Gamma/2$, from (5.4). The inverse temperature $\beta = -k^2$ is an eigenvalue given by

$$\beta_{nm} = -k_{nm}^2 = -\pi\alpha_{nm}^2 \tag{5.12}$$

where α_{nm} denotes the mth zero of the Bessel function J_n. Their amplitude C can be computed from the energy constraint (5.7). In the case of the fundamental mode $(n, m) = (1, 1)$, we find

$$C = \pm\frac{2H^{1/2}}{k_{11}J_0(\alpha_{11})}$$

in terms of the parameter H defined in (5.10). Finally, the entropy can be simply written as

$$\mathscr{S}_{nm} = \beta_{nm}H. \tag{5.13}$$

For $(n, m) = (1, 1)$ the solution is formed by two vortices of opposite sign, and we recover the dipole structure studied in the rectangular domain (§4). However, in the laboratory frame ($\mathscr{R}$), this structure is no longer stationary in general, but rotates about the origin with angular velocity Ω and, for high values of Ω, looks like a decentred monopole.

(ii) The continuum solutions are axisymmetric (monopole) and can be expressed in terms of Bessel functions of the form (see Appendix B):

$$\psi' = \frac{\Gamma'}{2\pi\alpha}\left(\frac{J_0(kr)}{J_1(\alpha)} - \frac{J_0(\alpha)}{J_1(\alpha)}\right) \tag{5.14}$$

where $\alpha = k/\pi^{1/2}$, and exist for all the values of A. Their relative circulation is given by (5.6) which yields:

$$\Gamma' = 2\pi\frac{J_1(\alpha)}{J_3(\alpha)}\left(\frac{\Gamma}{2\pi} - L\right) \tag{5.15}$$

from which we can compute the angular velocity Ω by (5.4). Their temperature (or parameter α) can be then related to the control parameter A with the aid of the constraints (5.6) and (5.7). The final result (see Appendix B) is an equation of state of the form

$$J_3^2(\alpha) = A^2\left(\tfrac{2}{3}J_2^2(\alpha) - J_1(\alpha)J_3(\alpha)\right). \tag{5.16}$$

Like in §§3 and 4, this equation exhibits several solutions that must be classified according to their entropy

$$\mathscr{S} = \beta H\left(1 + \frac{A^2}{3}\frac{J_1(\alpha)}{J_3(\alpha)}\right) \tag{5.17}$$

computed from (5.8) and (5.14). As mentioned above, these solutions are obtained for $\beta = -k^2 \leqslant 0$. This condition corresponds to $\Lambda^2 \leqslant 2$, obtained by the development of $J_n(\alpha)$ in (5.16) in the limit $\alpha \to 0$ (i.e. $k \to 0$). The case of positive temperatures can be deduced from the previous one by performing the transformation $k \to ik$ and using $J_n(it) = i^n I_n(t)$ where $I_n(t)$ is the modified Bessel function of order n. For $\beta \to +\infty$, we find that $\Lambda^2 \to 3$ which is an upper bound for the control parameter.

(iii) The mixed solutions (monopole+dipole) are of the form

$$\psi' = \frac{\Gamma'}{2\pi\alpha}\left(\frac{J_0(kr)}{J_1(\alpha)} - \frac{J_0(\alpha)}{J_1(\alpha)}\right) + CJ_n(kr)\sin(n\theta + \delta) \tag{5.18}$$

with $n \neq 0$ and where Γ' is still given by (5.15). These solutions exist for $0 \leqslant \Lambda \leqslant \Lambda'_{nm}$ and their inverse temperatures $\beta = -k^2$ are the eigenvalues (5.12). The constant C can be computed from (5.6) and (5.7) as a function of the control parameter. For $\Lambda = 0$ we recover (5.11); for $\Lambda = \Lambda'_{nm}$, defined by introducing $\alpha = \alpha_{nm}(n \neq 0)$ in (5.16), we have $C = 0$ and we recover (5.14). For the dipole $(n, m) = (1, 1)$, we find explicitly

$$C = \pm\frac{2H^{1/2}}{kJ_0(\alpha_{11})}\left(1 - \frac{\Lambda^2}{\Lambda'^2_{11}}\right)^{1/2}$$

with $\Lambda'^2_{11} = 24/\alpha^2_{11}$.

For $0 \leqslant \Lambda \leqslant \Lambda'_{nm}$ a competition occurs between solutions (5.14) and (5.18). To select the most probable structure, we have to compare their entropy, given by (5.17) in both cases. For $\Lambda = 0$, we find for the monopole

$$\mathscr{S}^{(m)} = -\pi\alpha^2_{31}H \tag{5.19}$$

and for the dipole

$$\mathscr{S}^{(d)} = -\pi\alpha^2_{11}H. \tag{5.20}$$

Since $\alpha_{31} \simeq 6.38$ and $\alpha_{11} \simeq 3.83$, the dipole is found to have a higher entropy than the corresponding monopole (see figure 7) and will be selected in the equilibrium as the most probable state. These conclusions still hold in the whole range $0 \leqslant \Lambda \leqslant \Lambda'_{nm}$. The tripole solutions, i.e. the mixed modes at $\beta = \beta_{21}$, have also an entropy higher than the monopole for sufficiently small Λ, but it is always dominated by the dipole in our linearized approximation. The considerations of §3.5 can be readily extended to the circular case, and the mode with the highest entropy, the dipole or monopole depending on Λ, appears to be the only entropy maximum: all the other modes are not even local maxima.

This conclusion is in agreement with previous investigations of maximum-entropy states in a disk by Smith & O'Neil (1990) and Chen & Cross (1994). They find indeed either axisymmetric or dipolar structures in the ranges of parameters they have considered. Whitaker & Turkington (1994) obtain a tripolar structure, but with a high-energy state involving little mixing, for which our analysis clearly fails. The parameter range covered by these studies is limited, and our analytical results provide a useful complement for the limit of strong mixing, as well as a general understanding of the problem. It then appears from these different studies that the axisymmetric, dipolar and tripolar structures are most probably the only possible states of maximum entropy in the disk. This indeed corresponds to the different structures observed in the laboratory experiments on self-organization by Denoix, Sommeria & Thess (1994). We can conclude from the present analysis that the tripole can only be observed with a strongly nonlinear $\omega - \psi$ relationship. Otherwise it is not an entropy maximum, although it is a possible solution of (2.12) with the right constraints.

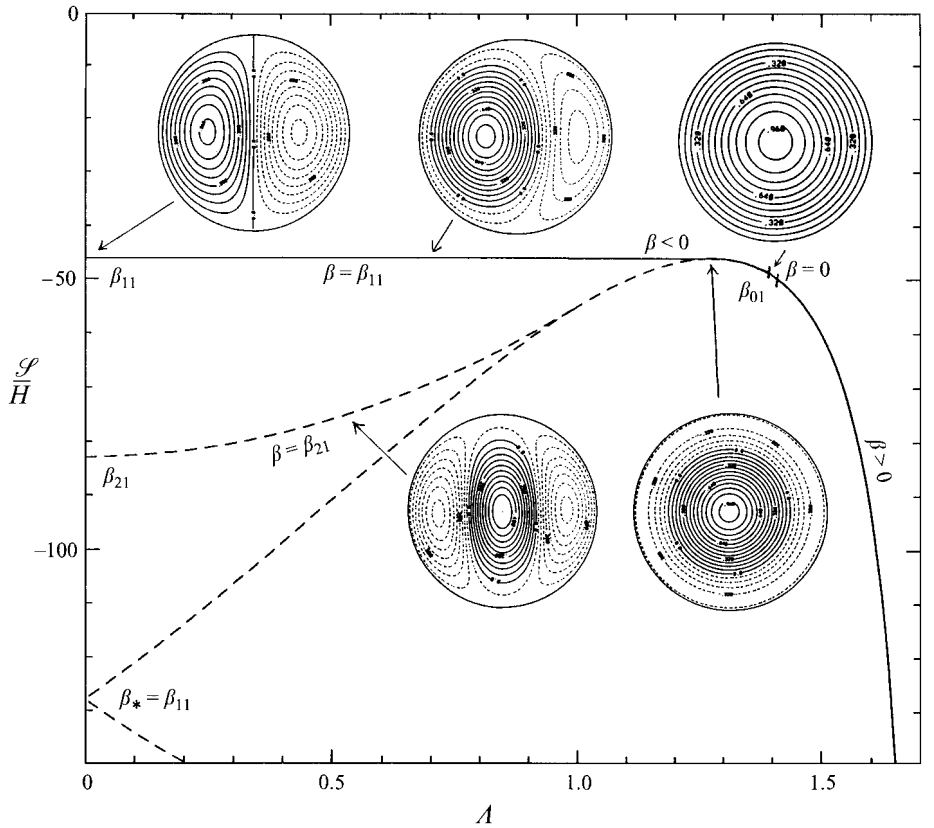

FIGURE 7. Same as figure 5 but for the circular domain. The mixed solution has the highest entropy along the line $\beta = \beta_{11} \equiv -k_{11}^2 = -46.12$, and joins continuously the monopole solution for $A = A'_{11} = 1.28$. The tripole (line $\beta = \beta_{21} \equiv -k_{21}^2 = -82.86$) has a lower entropy, as does the monopole for $A < 1.28$.

6. Comparison with a minimum-enstrophy principle

Selective decay (minimum-enstrophy) empirical principles have been proposed to explain self-organization in two-dimensional turbulence. Such principles have been found useful in some cases, but without clear physical support. The predictions also disagree in many cases with computations or laboratory experiments. However, we shall show in this section that a form of minimum-enstrophy principle is recovered by the statistical theory in the limit of strong mixing. This provides therefore a justification of this principle from the Euler equations, while specifying its range of validity.

The justification of a selective decay principle is often given in term of weak viscous effects: the enstrophy tends to cascade toward small scales where it is dissipated, while energy remains trapped to large scales. The conserved quantities of inviscid motion are classified into two groups: the 'dissipated integrals' (like enstrophy) which undergo turbulent cascades and decay even with a small viscosity, and the 'rugged integrals' (like energy) which remain constant in the limit of small viscosity. This property has suggested a general organization principle, stating that the final flow would minimize enstrophy with the constraint of a given energy, and possibly the constraint of other rugged integrals (see e.g. Hasegawa 1985).

Nevertheless a general justification in terms of viscous effects leads to physical

contradictions. Indeed a good experimental example of two-dimensional turbulence is provided by electron plasmas, for which the vorticity is proportional to the electron density and must of course remain positive. However the minimum-enstrophy state involves in general both *negative and positive vorticity*, and some *ad hoc* restriction of positivity must be added. By contrast the maximum entropy prediction always preserves the distribution of vorticity levels, so that no spurious negative vorticity appears. The selective decay hypothesis has been found most useful in quasi-geostrophic flows over topography (Bretherton & Haidvoguel 1976), where the vorticity is replaced by the potential vorticity. This quantity is conserved and stirred by the inviscid dynamics in the same way as vorticity in the Euler systems. The state of minimum potential enstrophy for a given energy appears to be selected. This principle cannot be justified by viscous effects, as they keep the same form as in the two-dimensional Navier–Stokes equations: they would still dissipate the enstrophy, not the potential enstrophy. Therefore the self-organization of two-dimensional turbulence is essentially an inertial process, and *viscous effects cannot provide a general principle of organization.*

In this context of quasi-geostrophic flows over topography, the state of minimum potential enstrophy has been also justified as a statistical equilibrium of (inviscid) truncated spectral models (Carnevale & Frederiksen, 1987): these states tend to the state of minimum potential enstrophy when the truncation wavenumber tends to infinity. Fluctuations are then mostly at very small scales and contain negligable energy. However truncated spectral models do not predict any mean flow in the absence of topography (furthermore the truncation breaks many conservation laws, leaving only the enstrophy and energy as conserved quantities).

The point of view of our statistical theory is that part of the initial enstrophy Γ_2 is irreversibly transferred into fine-grained (microscopic) vorticity fluctuations, so that the final coarse-grained enstrophy, calculated from the field of locally averaged vorticity

$$\Gamma_2^{c.g} = \int \overline{\omega}^2 \mathrm{d}^2\boldsymbol{r} \tag{6.1}$$

is smaller than Γ_2. This is physically similar to the situation described by Carnevale & Frederiksen (1987) with spectral models, but the formalism is now quite different, with a much wider range of applicability. In the presence of a small viscosity, we can assume that the fine-grained fluctuations are eventually smoothed out (their enstrophy is dissipated), leaving only the steady flow with the vorticity field $\overline{\omega}(\boldsymbol{r})$. Notice that such viscous smoothing is passive (like in usual theories of turbulent inertial range), and *does not control* the flow organization. The result is an enstrophy decay for constant energy, but without reaching the minimal-enstrophy state in general.

We can however justify a minimum-enstrophy principle in our limit of strong mixing. The mere minimization of enstrophy with given energy clearly yields the first eigenmode of the Laplacian in all cases, unlike our calculations. However we recover our results by further assuming that the circulation Γ is also a rugged integral, hence an additional constraint in the minimization problem. Let us minimize the coarse-grained enstrophy $\Gamma_2^{c.g.}$, with a given energy E and circulation Γ, leading to the condition for the first variations

$$\delta\Gamma_2^{c.g.} - \lambda\delta E - \mu\delta\Gamma = 0 \tag{6.2}$$

where λ and μ are Lagrange multipliers. This leads again to the linear relationship (2.13) between vorticity and stream function, as in the strong mixing limit of the

statistical theory. Therefore the same branches of solutions are obtained. The solution with the lowest enstrophy must be selected, and it appears to be also the solution with the highest entropy. Indeed, expressing the equilibrium vorticity as in (2.13), we get from (2.16)

$$\Gamma_2^{c.g} = \Gamma^2 - 2\mathscr{S}. \tag{6.3}$$

Thus the minimum enstrophy principle in the form (6.2) *gives the same results as the statistical theory in the limit of strong mixing.* A similar conclusion is drawn for the circular domain, considering the angular momentum as a rugged integral, *in addition* to the circulation. Of course this correspondence no longer holds, for higher energy, when linearization is longer more valid.

7. Conclusions

We have obtained general expressions for maximum-entropy states when the argument $(\tilde{\beta}\sigma\psi)$ in (2.9) is small, so that the relevant relations can be linearized. The results have been generally expressed in terms of the eigenmodes of the Laplacian, and the particular cases of a rectangular and circular domains have been developed. In this linear approximation, our statistical theory justifies a form of minimum-enstrophy principle, considering the circulation as a rugged integral, in addition to energy. The limitations of this principle are clearly found by considering the higher-order expansion (see Appendix A and §4.2).

This approximation is valid in a limit of strong mixing, near the maximum of the curve $S(E)$. The range of validity appears to be remarkably large (it is in fact sufficient that $\tilde{\beta}\sigma\psi \sim 1$), as indicated by the comparision of the approximate entropy (2.16) with the exact value (figure 1), and also in the discussion of §4.2.

In a square domain, we correctly predict an organization into a monopole, observed in numerical simulations and laboratory experiments. We also predict a transition to a dipole when the domain becomes slightly rectangular, and this is in agreement with preliminary tests. In the circular domain, we predict an axisymmetric or dipolar state, depending on the integral constraints. Tripoles are also solutions of the linearized equation (5.5), but are excluded as not entropy maxima. We therefore conclude that tripoles can only exist with a strongly nonlinear relationship between vorticity and stream function.

The present procedure can be readily applied to other geometries, and also to geophysical models involving the multi-level quasi-geostrophic equations, and it provides a quite interesting approach to these problems. The first reason is of course that equation (2.12) determining the flow structure can be linearized and analytically solved to a large extent. More importantly however, the results in this limit of strong mixing depend only on a single control parameter A instead of the whole distribution of vorticity levels. This allows a general understanding of the problem, and a classification of the equilibrium states. By pushing the expansion to higher order in energy, the influence of the successive moments of the vorticity probability distribution can be understood. For a symmetric distribution in positive and negative vorticity, the kurtosis Ku determines the deviation to the linear relationship (see (A12)): if, in addition $\langle\psi\rangle = 0$, the $\omega - \psi$ relationship behaves like a tanh function when $Ku < 3$ and like a sinh function when $Ku > 3$ (for instance with an initial condition involving compact vortices). The opposite limit of maximum energy, for a given vorticity probability distribution (as computed by Carnevale & Vallis 1990), is also a quite useful complement to the understanding of the structure of the problem. The full

exploitation of the statistical theory requires however the numerical resolution of the general equation (2.12), joining these two limits with increasing energy, as performed for instance by Turkington & Whitaker (1995) or Juttner *et al.* (1995).

We must stress that this theory, unlike previous ones, provides a well-defined prediction for the final flow organization in all cases, consistent with the properties of the Euler equations. This fact can be clearly understood in our limit of strong mixing. In particular it is remarkable that most solutions of equation (2.13) can be eliminated as not entropy maxima, even in a local sense, as shown in §3.5: only the solution with the maximum entropy (or minimum coarse-grained enstrophy) is selected, (with possibly also a second, metastable, state).

Testing the range of validity of this statistical theory requires an extensive survey of examples, beyond the scope of the present paper. A prerequisite for such a systematic comparison is of course to be able to calculate and understand the predictions of the statistical theory with general distributions of vorticity levels. This is not an easy untertaking, and the present paper contributes to it. Some comparisons have already been discussed in §4.2, as well as in Juttner *et al.* (1995), and references herein. A good agreement has been obtained when a final state is reached by rapid stirring. Efficient stirring is limited to regions with strong vorticity, while transfers towards small scales by straining effects dominate in the surrounding background. This leads to some discrepancies in the statistical theory (Denoix *et al.* 1994), whose effects tend to cumulate when the evolution towards the final state takes a longer time. Boundary layer detachment is another source of discrepancy, feeding the flow with vorticity sheets emitted by the boundary layers (e.g. Sommeria 1988; van Heijst *et al.* 1990). It is not known to what extend such discrepancies would persist in the limit of an inviscid flow. Yet the statistical equilibrium is an ideal limit, quite useful as a framework to study self-organization. As a second step, restrictions to complete stirring can be introduced in the form of kinetic equations, describing relaxation towards statistical equilibrium. This approach is developed by Robert & Rosier (1996), and by Kazantsev, Sommeria & Verron (1995) for oceanic currents.

Notice finally that the present paper provides a set of steady solutions of the Euler equation for any given energy and circulation (and angular momentum in the disk case). This can be useful even without any reference to the underlying statistical theory.

This work is part of a continuous collaboration with R. Robert and team of Laboratoire d'Analyse numérique at Université de Lyon. We have benefited from many discussions with this group, especially on mathematical aspects. We thank B. Juttner for kindly providing figure 1 and N. Whitaker for his helpful collaboration.

Appendix A. The strong mixing expansion

When the parameter $\tilde{\beta}\sigma\psi$ is small, we can expand the basic equations in powers of this quantity. This expansion must be carried out directly to order 1 for the stream function (because the zero-order term vanishes for zero circulation), and to order 2 for the energy and the entropy. As a result, (2.9) (2.10) and (2.11) must be written in the approximate form

$$Z \simeq 1 - A_1\tilde{\beta}\psi + \tfrac{1}{2}A_2(\tilde{\beta}\psi)^2, \tag{A 1}$$

$$\rho(\boldsymbol{r},\sigma) \simeq g(\sigma)\left\{1 + (A_1 - \sigma)\tilde{\beta}\psi + \tfrac{1}{2}(\sigma^2 - 2A_1\sigma + 2A_1^2 - A_2)(\tilde{\beta}\psi)^2\right\}, \tag{A 2}$$

$$\overline{\omega} = -\Delta\psi \simeq A_1 + (A_1^2 - A_2)\tilde{\beta}\psi, \tag{A 3}$$

where the different moments of the function $g(\sigma)$ are denoted by

$$A_n = \int g(\sigma)\sigma^n \mathrm{d}\sigma \qquad (n \neq 0) \tag{A 4}$$

(we have set $A_0 = 1$, without loss of generality). The Lagrange multipliers $g(\sigma)$ must be related to the global vorticity distribution $\gamma(\sigma)$ thanks to the integral condition (2.5) that expands to

$$\gamma(\sigma) \simeq g(\sigma)\left\{1 + (A_1 - \sigma)\tilde{\beta}\langle\psi\rangle + \tfrac{1}{2}(\sigma^2 - 2A_1\sigma + 2A_1^2 - A_2)\tilde{\beta}^2\langle\psi^2\rangle\right\} \tag{A 5}$$

where $\langle\rangle = \int \mathrm{d}^2\boldsymbol{r}$ denotes the average over the whole surface ($\mathscr{D}$). Equation (A5) can be reversed to give

$$g(\sigma) \simeq \gamma(\sigma)\left\{1 - (A_1 - \sigma)\tilde{\beta}\langle\psi\rangle + (A_1 - \sigma)^2\tilde{\beta}^2\langle\psi\rangle^2 - \tfrac{1}{2}(\sigma^2 - 2A_1\sigma + 2A_1^2 - A_2)\tilde{\beta}^2\langle\psi^2\rangle\right\}. \tag{A 6}$$

Combining equations (A4) and (A6) we obtain to order 1

$$A_n \simeq \Gamma_n - (A_1\Gamma_n - \Gamma_{n+1})\tilde{\beta}\langle\psi\rangle \tag{A 7}$$

To order 1 for A_1 and order 0 for A_2, we have

$$A_1 \simeq \Gamma + (1 - \Gamma^2)\tilde{\beta}\langle\psi\rangle \tag{A 8}$$

$$A_2 \simeq 1 \tag{A 9}$$

Substituting in (A3) yields equation (2.13) for the stream function, with the correspondence (2.15) between β and $\tilde{\beta}$.

Expressing $\ln\rho(\boldsymbol{r},\sigma)$ by (2.9), we write the entropy (2.7) as a function of the conserved quantities and their canonical Lagrange multipliers:

$$S = 2\tilde{\beta}E + \int \tilde{\alpha}(\sigma)\gamma(\sigma)d\sigma + \int \ln Z \, \mathrm{d}^2\boldsymbol{r} \tag{A 10}$$

Using (A6), (A8) and (A1) we expand $\tilde{\alpha}(\sigma) = -\ln g(\sigma)$ and $\ln Z$ to order 2 and eventually find (2.16).

The expansion can be pushed to higher order by a similar method. We need to go directly to order 4, since the term of order 3, related to the circulation, is small (of the same order as the term of order 4). This yields the equation for the new stream function ψ:

$$-\Delta\psi = B_0 + B_1\psi + B_2\psi^2 + B_3\psi^3 \tag{A 11}$$

where

$$B_2 = \tfrac{1}{2}\tilde{\beta}^2\left\{(\Gamma_4 - 3\Gamma_2^2 - 4\Gamma\Gamma_3 + 6\Gamma^2\Gamma_2)\,\tilde{\beta}\langle\psi\rangle + (\Gamma_3 - 3\Gamma\Gamma_2 + 2\Gamma^3)\right\},$$

$$B_3 = -\tfrac{1}{6}\tilde{\beta}^3\,(\Gamma_4 - 3\Gamma_2^2 - 4\Gamma\Gamma_3 + 12\Gamma^2\Gamma_2 - 6\Gamma^4)$$

(we have kept Γ_2 for clarity, but Γ_2=1 with our choice of units, and $\Gamma_1 \equiv \Gamma$). The terms in B_2 and B_3 are small corrections in (A11), and can be expressed with the first order solutions and inverse temperature $\tilde{\beta}$. Equation (A11) then becomes a

Helmholtz equation for the corrected function ψ, with a right-hand term given by the solution at previous order. The unknown coefficients B_0 and B_1 are then obtained by the constraints on energy and circulation, like in (2.13).

In the case of a symmetric distribution in positive and negative vorticity, we have $\Gamma_{2n+1} = 0$ and equation (A11) reduces to:

$$-\Delta\psi = B_0 + B_1\psi + \frac{\tilde{\beta}^3}{2\Gamma_2^2}(Ku-3)\langle\psi\rangle\psi^2 - \frac{\tilde{\beta}^3}{6\Gamma_2^2}(Ku-3)\psi^3 \tag{A 12}$$

where $Ku = \Gamma_4/\Gamma_2^2$ is the kurtosis.

Appendix B. The equations of state $\beta(\Lambda)$

In this section, we give the main steps for deriving the relationship between the inverse temperature β and the control parameter Λ in the case of an arbitrary domain with no specific symmetry (equation (3.7)) and in the case of a circular domain (equation (5.16)).

B.1. *Arbitrary domain with no specific symmetry*

The inverse temperature β is determined by the energy constraint (2.14) that we can write as a function of ϕ_β, defined by (3.4), in the form

$$(1-\beta\langle\phi_\beta\rangle)^2 = \Lambda^2(\langle\phi_\beta\rangle - \beta\langle\phi_\beta^2\rangle). \tag{B 1}$$

The mean values of ϕ_β and ϕ_β^2 can be expanded in series with the aid of (3.6). Using the orthonormality of ψ_n, we find

$$\langle\phi_\beta\rangle = \sum_n \frac{\langle\psi_n''\rangle^2}{\beta-\beta_n''} \tag{B 2}$$

$$\langle\phi_\beta^2\rangle = \sum_n \frac{\langle\psi_n''\rangle^2}{(\beta-\beta_n'')^2} = -\frac{\mathrm{d}}{\mathrm{d}\beta}\langle\phi_\beta\rangle \tag{B 3}$$

The Fourier series (3.6) converges to a quadratic norm in $\mathscr{L}^2(\mathscr{D})$, so that (B2) and (B3) converge. If we now introduce the function $F(\beta)$ defined by (3.8), it is easy to show from (B3) and (B2) that its derivative is given by

$$F'(\beta) = \langle\phi_\beta\rangle - \beta\langle\phi_\beta^2\rangle = -\sum_n \frac{\beta_n''\langle\psi_n''\rangle^2}{(\beta-\beta_n'')^2} > 0 \tag{B 4}$$

so that (B1) takes the simple form (3.7).

B.2. *The case of a circular domain*

The general solution of Helmholtz equation (5.5) can be expanded on the basis of the eigenmodes of the Laplacian:

$$\psi' = \epsilon_0 + \sum_n a_n J_n(kr)\sin(n\theta+\delta_n) \tag{B 5}$$

where $\epsilon_0 = \langle\psi'\rangle - \Gamma'/k^2$ is a particular solution and J_n is a Bessel function of order n. We have excluded Neumann functions because they would lead to divergencies in the core of the vortex ($r \to 0$). The boundary condition forbids any angular variation

of ψ' so that, if we assume that $\alpha \equiv k/\pi^{1/2}$ is not a zero α_{nm} of a Bessel function, equation (B5) reduces to

$$\psi' = \epsilon_0 \left(1 - \frac{J_0(kr)}{J_0(\alpha)}\right). \tag{B 6}$$

Taking the average $\langle\rangle$ and eliminating $\langle\psi'\rangle$ yields the result (5.14). The inverse temperature β, or the equivalent parameter α, and the angular speed Ω (related to the relative circulation Γ' by (5.4)), are determined by the constraints (5.6) and (5.7) for the energy E and the angular momentum L. If we substitute the result (5.14) in these constraints, we obtain the following system for α and Γ':

$$L = \frac{\Gamma'}{2\pi}\left(1 - \frac{4}{\alpha}\frac{J_2(\alpha)}{J_1(\alpha)}\right) + \frac{\Gamma}{2\pi}, \tag{B 7}$$

$$E = \frac{3\Gamma'^2}{16\pi}\left(1 - \frac{4}{\alpha}\frac{J_2(\alpha)}{J_1(\alpha)} + \frac{2J_2^2(\alpha)}{3J_1^2(\alpha)}\right) - \frac{\Gamma\Gamma'}{16\pi}\left(1 - \frac{4}{\alpha}\frac{J_2(\alpha)}{J_1(\alpha)}\right) - \frac{\Gamma L}{8} + \frac{\Gamma^2}{8\pi}. \tag{B 8}$$

Solving for Γ' in (B7) and substituting in (B8) yields the results (5.15) and (5.16). Working similarly on the entropy (5.8) leads to (5.17).

In fact, we can come to these equations more rapidly if we notice that the quantities $\mathcal{A}$ and H are invariant under a solid rotation. It is then possible to carry out the previous study in a frame of reference ($\mathscr{R}_*$) where Γ vanishes and use the invariance of $\mathcal{A}$ and H to recover (5.15), (5.16) and (5.17) in the general case. Notice by the way that in ($\mathscr{R}_*$) we have $H = E_* > 0$ so that H is positive in any frame.

Appendix C. General features of the bifurcation diagram

In order to understand the behaviour of (3.7), we need to study the functions $F^2(\beta)$ and $F'(\beta)$, represented in figure 8. From the series expansion (B4) we have that $F' > 0$ (since $\beta_n'' < 0$), so that the function F is strictly increasing on each interval on which it is defined: $]\beta_{n+1}'', \beta_n''[$ and $]\beta_1'', +\infty[$. The asymptotic behaviour near each of the eigenvalues β_n'' is given by keeping only the divergent term in $\beta - \beta_n''$ in the series expansions (B2) and (B4). It appears therefore that $F(\beta) \to -\infty$ when $\beta \to \beta_{n+1}''^{+}$ and $F(\beta) \to +\infty$ when $\beta \to \beta_n''^{-}$, so that F strictly increases from $-\infty$ to $+\infty$ in each interval $]\beta_{n+1}'', \beta_n''[$. As a consequence, there is a single root $\beta_*^{(n)}$ for which $F(\beta_*^{(n)}) = 0$ in this interval. These roots $\beta_*^{(n)}$ are solutions of (3.7) for $\mathcal{A} = 0$, and are therefore in competition with the eigenmode solutions ψ_n' discussed in §3.1.

It is useful to follow these solutions as $\mathcal{A}^2$ increases from 0. For small $\mathcal{A}^2$, the pair of solutions (3.9) is obtained on each side of each root $\beta_*^{(n)}$. These are denoted $\beta^{(n-)}$ and $\beta^{(n+)}$ respectively in figure 8. As $\mathcal{A}^2$ increases, the solution $\beta^{(n-)} < \beta_*^{(n)}$ in the interval $]\beta_{n+1}'', \beta_n''[$ decreases, while the solution $\beta^{((n+1)+)} > \beta_*^{(n+1)}$ in the interval $]\beta_{n+2}'', \beta_{n+1}''[$ increases, so they eventually join at $\beta = \beta_{n+1}''$. This junction is smooth, as seen from the asymptotic limit of (3.7) as $\beta \sim \beta_{n+1}''$. Indeed, from the asymptotic behaviour of $F(\beta)$ and $F'(\beta)$, given by the divergent term in the series expansions (B2) and (B4), (3.7) becomes $\mathcal{A}^2 \simeq -\beta_{n+1}''\langle\psi_{n+1}''\rangle \equiv \mathcal{A}_{n+1}''^2$ (see equation (3.3)) on each side of the asymptote $\beta = \beta_{n+1}''$. Therefore the corresponding solutions tend smoothly to the eigenmode (3.2).

We now discuss the solutions for $\beta > \beta_1''$. In the limit $\beta \to +\infty$, (3.5) yields $\phi_\beta \sim 1/\beta$, except in boundary layers where the Laplacian in (3.5) is dominated by the derivatives with respect to the coordinate ζ normal to the boundary ($\partial\mathscr{D}$). Therefore (3.5) is only ζ-dependent, and its solution (consistent with the boundary conditions

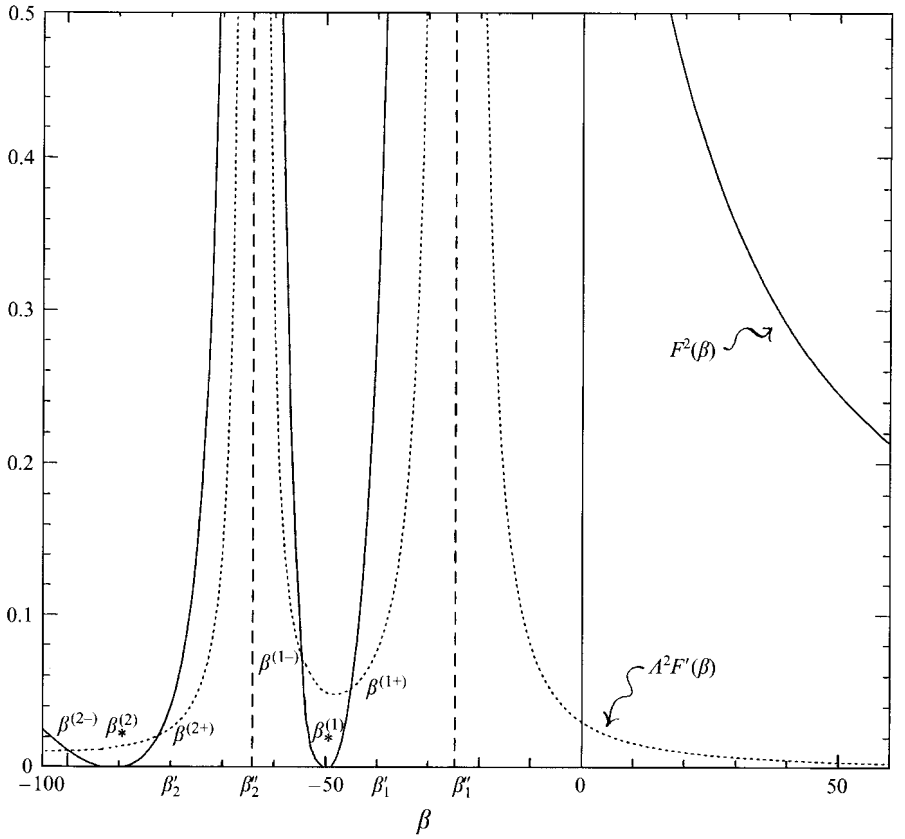

FIGURE 8. Graph of the functions F^2 (solid line) and F' (dotted line) versus β, where F is the function defined by (3.8) and (3.5). The computations are performed for the rectangular domain with aspect ratio 2, but the qualitative behaviour is general, as discussed in the text. The two functions diverge at the eigenvalues of the Laplacian, corresponding to an eigenmode with non-zero mean, β''_1, β''_2... The pair of solutions $\beta^{(1-)}$ and $\beta^{(1+)}$ of (3.7), around the first zero $\beta^{(1)}_*$ of F, is represented, as well as the similar pair around the second zero $\beta^{(2)}_*$.

$\phi_\beta = 0$ for $\zeta = 0$) is simply

$$\phi_\beta = \frac{1}{\beta}\left(1 - \mathrm{e}^{-\beta^{1/2}\zeta}\right). \tag{C 1}$$

Denoting the perimeter of the domain by $\mathscr{P}$, (3.8) and (B4) yield respectively

$$F(\beta) \sim -\frac{\mathscr{P}}{\beta^{1/2}} \quad \text{and} \quad F'(\beta) \sim \frac{\mathscr{P}}{2\beta^{3/2}}. \tag{C 2}$$

Therefore $F(\beta) \to 0^-$ when $\beta \to +\infty$. Thus F strictly increases from $-\infty$ to 0^- on the interval $]\beta''_1, +\infty[$, so that it remains strictly negative, and (3.7) has no solution on this interval for $\Lambda^2 \to 0$. For large values of Λ^2, there is always a solution corresponding to the limit of large β, deduced by introducing (C2) into (3.7):

$$\beta \simeq \frac{\Lambda^4}{2\mathscr{P}}. \tag{C 3}$$

Coming back to the stream function ψ, using (3.4), (3.8), (C1) and (C2), we find

$$\beta\psi \sim \frac{\Gamma^3}{E(2\mathscr{P})^{3/2}}$$

and this quantity must remain small for the linear approximation to be valid. This approximation is therefore satisfied in the limit of strong mixing, as long as A remains finite, or at least if it tends to infinity with $A^2\Gamma << 1$.

REFERENCES

BRETHERTON, F. P. & HAIDVOGUEL, D. B. 1976 Two-dimensional turbulence over topography. *J. Fluid Mech.* **78**, 129–154.

CARNEVALE, G. F. & FREDERIKSEN, J. S. 1987 Nonlinear stability and statistical mechanics of flow over topography. *J. Fluid Mech.* **175**, 157–181.

CARNEVALE, G. F. & VALLIS, G. K. 1990 Pseudo-advective relaxation to stable states of inviscid two-dimensional fluids. *J. Fluid Mech.* **213**, 549–571.

CHAPLYGIN, S. A. 1902 One case of vortex motion in fluid *Proc. Phys. Sec. Natural Phil. Soc.* **11**, 114.

CHAVANIS, P. H. & SOMMERIA, J. 1995 Classification of self-organized isolated vortices in two-dimensional turbulence. In preparation.

CHEN, P. & CROSS, M. C. 1994 Phase diagram for coherent vortex formation in the two-dimensional inviscid fluid in circular geometries. *Phys. Rev.* E **50**, 2022–2029.

DENOIX, M. A., SOMMERIA, J. & THESS A. 1994 Two-dimensional turbulence: the prediction of coherent structures by statistical mechanics. In *Progress in Turbulence Research* (ed. H. Branover & Y. Unger), pp. 88–107. AIAA.

FOFONOFF, N. P. 1954 Steady flow in a frictionless homogeneous ocean. *J. Mar. Res.* **13**, 254–262.

HASEGAWA, A. 1985 Self-organization processes in continuous media *Adv. Phys.* **34**, 1–42.

HEIJST, VAN, G. J. F., DAVIES, P. A. & DAVIS, R. G. 1990 Spin-up in a rectangular container *Phys. Fluids* A **2**, 150–159.

JOYCE, G. & MONTGOMERY, D. 1973 Negative temperature states for the two-dimensional guiding-centre plasma. *J. Plasma Phys.* **10**, 107–121.

JUTTNER, B., THESS, A. & SOMMERIA, J. 1995 On the symmetry of self-organized structures in two-dimensional turbulence, *Phys. Fluids* **7**, 2108–2110.

KAZANTSEV, E., SOMMERIA, J. & VERRON, J. 1995 Subgridscale eddy parametrisation by statistical mechanics in a barotropic ocean model. *J. Phys. Oceanogr.* (submitted).

KRAICHNAN, R. H. & MONTGOMERY, D. 1980 Two-dimensional turbulence *Rep. Prog. Phys.* **43**, 547–617.

KUZ'MIN, G. A. 1982 Statistical mechanics of the organisation into two-dimensional coherent structures. In *Structural Turbulence* (ed. M. A. Goldshtik), pp. 103–114. Acad. Naouk CCCP Novosibirsk, Institute of Thermophysics.

LYNDEN-BELL, D. 1967 Statistical mechanics of violent relaxation in stellar systems. *Mon. Not. R. Astron. Soc.* **136**, 101–121

MARTEAU, D., CARDOSO, O. & TABELING, P. 1995 Equilibrium states of 2D turbulence: an experimental study. *Phys. Rev.* E **51**, 5124–5127.

MICHEL, J. & ROBERT, R. 1994 Large deviations for Young measures and statistical mechanics of infinite dimensional dynamical systems with conservation law. *Commun. Math. Phys.* **159**, 195–215.

MILLER, J. 1990 Statistical mechanics of Euler equations in two dimensions. *Phys. Rev. Lett.* **65**, 2137–2140.

MILLER, J., WEICHMAN, P. B. & CROSS, M. C. 1992 Statistical mechanics, Euler's equation and Jupiter's Red Spot. *Phys. Rev.* A **45**, 2328–2359.

MONTGOMERY, D. & JOYCE, G. 1974 Statistical mechanics of negative temperature states. *Phys. Fluids* **17**, 1139–1145.

MONTGOMERY, D., MATTHAEUS, W., STRIBLING, W., MARTINEZ, D. & OUGHTON, S. 1992 Relaxation in two dimensions and the sinh-Poisson equation. *Phys. Fluids* A **4**, 3–6.

ONSAGER, L. 1949 Statistical hydrodynamics. *Nuovo Cimento Suppl.* **6**, 279–287.

POINTIN, Y. B. & LUNDGREN, T. S. 1976 Statistical mechanics of two-dimensional vortices in a bounded container. *Phys. Fluids* **19**, 1459–1470.

ROBERT, R. 1990 Etat d'équilibre statistique pour l'écoulement bidimensionnel d'un fluide parfait. *C. R. Acad. Sci. Paris* **311** (I), 575–578.

ROBERT, R. 1991 Maximum entropy principle for two-dimensional Euler equations. *J. Statist. Phys.* **65**, 531–551.

ROBERT, R. & ROSIER, 1996 The modelling of small scales in 2D turbulent flows: a statistical mechanical approach. *J. Fluid Mech.* (submitted).

ROBERT, R. & SOMMERIA, J. 1991 Statistical equilibrium states for two-dimensional flows. *J. Fluid Mech.* **229**, 291–310.

SMITH, A. R. & O'NEIL, T. M. 1990 Nonaxisymmetric thermal equilibria of a cylindrically bounded guiding-center plasma or discrete vortex system. *Phys. Fluids* B **2**, 2961–2975.

SOMMERIA, J. 1986 Experimental study of the two-dimensional inverse energy cascade in a square box. *J. Fluid Mech.* **170**, 139–168.

SOMMERIA, J. 1988 Electrically driven vortices in a strong magnetic field. *J. Fluid Mech.* **189**, 139–168.

SOMMERIA, J. 1994 Organized vortices as maximum entropy structures. In *Modelling of Oceanic Vortices* (ed. G. J. F. van Heijst), pp. 37–50. North-Holland.

STERN, M. 1975 Minimal properties of planetary eddies. *J. Mar. Res.* **33**, 1–13.

THESS, A., SOMMERIA, J. & JUTTNER, B. 1994 Inertial organization of a two-dimensional turbulent vortex street *Phys. Fluids* **6**, 2417–2429.

TURKINGTON, B. & WHITAKER, N. 1995 Statistical equilibrium computations of coherent structures in turbulent shear layers. *SIAM J. Sci. Comput.* (to appear).

VERRON, J. & SOMMERIA, J. 1987 Numerical simulation of a two-dimensional turbulence experiment in magnetohydrodynamics. *Phys. Fluids* **30**, 732–739.

WHITAKER, N. & TURKINGTON, B. 1994 Maximum entropy states for rotating vortex patches. *Phys. Fluids* **6**, 3963–3973.